

Traj-MLLM: Can Multimodal Large Language Models Reform Trajectory Data Mining?

Shou Liu

liushuo22s@ict.ac.cn

University of Chinese Academy of
Sciences
China

Di Yao[†]

yaodi@ict.ac.cn

Institute of Computing Technology,
Chinese Academy of Sciences
China

Yan Lin

lyan@cs.aau.dk

Department of Computer Science,
Aalborg University
Denmark

Gao Cong

gaocong@ntu.edu.sg

College of Computing and Data
Science, Nanyang Technological
University
Singapore

Jingping Bi

bjp@ict.ac.cn

Institute of Computing Technology,
Chinese Academy of Sciences
China

Abstract

Building a general model capable of analyzing human trajectories across different geographic regions and different tasks becomes an emergent yet important problem for various applications. However, existing works suffer from the generalization problem, *i.e.*, they are either restricted to train for specific regions or only suitable for a few tasks. Given the recent advances of multimodal large language models (MLLMs), we raise the question: can MLLMs reform current trajectory data mining and solve the problem? Nevertheless, due to the modality gap of trajectory, how to generate task-independent multimodal trajectory representations and how to adapt flexibly to different tasks remain the foundational challenges. In this paper, we propose Traj-MLLM, which is the first general framework using MLLMs for trajectory data mining. By integrating multiview contexts, Traj-MLLM transforms raw trajectories into interleaved image-text sequences while preserving key spatial-temporal characteristics, and directly utilizes the reasoning ability of MLLMs for trajectory analysis. Additionally, a prompt optimization method is proposed to finalize data-invariant prompts for task adaptation. Extensive experiments on four publicly available datasets show that Traj-MLLM outperforms state-of-the-art baselines by 48.05%, 15.52%, 51.52%, 1.83% on travel time estimation, mobility prediction, anomaly detection and transportation mode identification, respectively. Traj-MLLM achieves these superior performances without requiring any training data or fine-tuning the MLLM backbones.

Keywords

Trajectory Data Mining, Multimodal Large Language Models

1 Introduction

Technical advances in GPS positioning enable the collection of world-wide human trajectory data derived from mobile devices [44], ride-hailing services [27], *etc.*. Trajectory data mining has become an increasingly important research topic, providing tools for numerous tasks such as travel time estimation [10, 34, 47], trajectory prediction [6, 47], anomaly detection [9, 23, 29], transportation mode identification [3, 11, 19], *etc.*. However, most works [6, 9, 23, 29]

are tailored to specific tasks and regions hindering their usage in real-world scenarios. Building a unified model capable of generalizing across different geographic regions and trajectory data mining tasks remains an emergent yet important problem.

In recent years, many efforts have been made to address this problem. These works can be categorized into two groups, *i.e.* trajectory foundation models and large language model (LLM)-based models. Methods in the first group [10, 31, 34] pre-train general trajectory representations on large-scale dataset and employ several learnable task heads for task adaptation. Due to the geographical heterogeneity, the learned representation models are only effective in trained regions and hard to extend to other data-scarce regions. For LLM-based models [30, 37, 41, 47], researchers attempt to utilize the generalization ability of LLMs for trajectory data mining. The LLMs are either treated as well-trained encoders directly feeding raw trajectories to obtain the task results [41] or fine-tuned to enhance traditional trajectory foundation models [30, 37, 47]. Nevertheless, LLMs struggle with handling numerical data and performing arithmetic operations[17], which limits their performances to encode raw trajectories. The commonly fine-tuned LLM is GPT-2[37, 47] which has only 1.5B parameters and exhibits limited generalization capability compared to modern, larger-scale models. Therefore, the generalization problem of trajectory data mining remains unsolved.

Notably, multimodal large language models (MLLMs) have shown remarkable reasoning ability, excelling in integrating multimodal information to enhance the performance of various tasks. The recent advances of MLLMs raise the question: can MLLMs reform current trajectory data mining and solve the generalization problem? Raw trajectories, recording as the sequences of GPS coordinates, are the simplified spatial-temporal expression of human movements. By projecting trajectories on the map, visual contextual information, such as POIs, road networks and traffic lights, can be represented in the visual modality. MLLMs' natural language processing (NLP) capability allows us to capture the regional information, human knowledge and task description with text. Moreover, well-trained MLLMs integrate rich common-sense knowledge and have strong generalization ability across different scenarios. It has significant

[†] Corresponding authors.

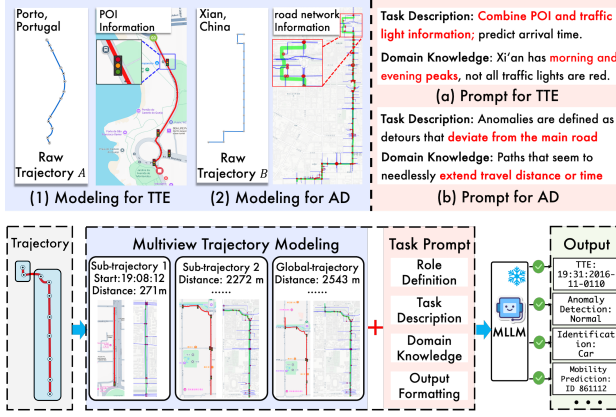


Figure 1: The motivation of Traj-MLLM.

potential to understand trajectories from visual and textual modalities without extra training and extend to analyze trajectories in unseen regions.

However, due to the modality gap of trajectory, two foundational challenges should be addressed to achieve region-agnostic and task-adaptive trajectory data mining with MLLMs:

- **Task-independent Trajectory Modeling.** The spatial-temporal characteristics vary a lot in trajectories and the required contextual information is heterogeneous for different tasks, leading to the challenge for modeling cross-region trajectories in a task-independent way. As shown in Figure 1, trajectories A and B are in different regions and A is much shorter than B. The information required for travel time estimation (TTE) is also different from anomaly detection (AD). Directly compressing all factors in one image would obscure real useful information leading to suboptimal performance. The trajectory modeling should not only capture the heterogeneity of all spatial-temporal and contextual information, but also extract region-agnostic features useful across different geographical regions.
- **Flexible Task Adaptation.** Instead of using trainable task heads for adaptation [47], we argue that textual prompts are more effective to activate the multimodal reasoning ability of MLLMs. The prompts can easily integrate human knowledge and define the reasoning steps for tasks clearly. As illustrated in Figure 1, the task descriptions, reasoning steps and output formats of TTE and AD are totally different. Nonetheless, these prompts should be easy to reference the information contained in trajectory modeling and data-invariant to meet the requirements of various tasks across different trajectory datasets. Therefore, it is challenging to construct task-specified prompts and achieve flexible task adaptation.

To address these challenges, we propose Traj-MLLM which is the first general framework that employs MLLMs for trajectory data mining. For unified trajectory modeling, we design a map-anchored tokenization mechanism which segments trajectories into sub-trajectories based on semantic completeness on the map. Both the visual and text representations are generated on the granularity of sub-trajectories. Taking these sub-trajectories as inputs, Traj-MLLM constructs different views of spatial scales and contextual factors that contain all required information for different tasks. For example, the trajectory A in Figure 1 is described at global

and sub-trajectory scales. The POIs and road networks information are modeled as the images and texts for each scale. Utilizing the multimodal reasoning ability of MLLMs, the temporal constraints are captured with the interleaved image-text sequences of visual and text representations. To achieve flexible task adaptation, we proposed a prompt optimization method that employs few seed trajectories and performs multi-round interactions with MLLMs to finalize the data-invariant task prompts. In usage, an arbitrary trajectory can be transformed into multimodal inputs of MLLMs to generate the analyzing results of various tasks.

By doing so, Traj-MLLM has three attractive benefits: (1) **Training-free.** Traj-MLLM relies on the reasoning ability of MLLMs to conduct trajectory data mining and does not need any data for model training or fine-tuning. This allows Traj-MLLM to be suitable for handling trajectories in arbitrary regions. (2) **Extensible.** Both the trajectory modeling and prompt optimization are general and independent, which makes Traj-MLLM extensible to new tasks by involving other information views and task prompts. (3) **Interpretable.** As the by-products, Traj-MLLM also outputs the reasoning process, which can be used to interpret the results.

The key contributions of this paper are summarized as follows:

- We propose a novel framework, namely Traj-MLLM, which employs MLLMs for region-agnostic and task-adaptive trajectory data mining. To the best of our knowledge, this is the first work to employ the reasoning ability of MLLMs to analyze human movement trajectories.
- To model trajectories in a unified way, we design a map-anchored mechanism to segment trajectories into sub-trajectories, and represent them in visual and text modalities, considering multiple views. For adapting to different tasks, a prompt optimization method is proposed to finalize data-invariant task prompts.
- Extensive experiments on four datasets demonstrate Traj-MLLM achieves significant performance improvements, i.e. 48.05%, 15.52%, 51.52%, 1.83% on four representative tasks, compared with state-of-the-art baselines. These results are achieved without any training.
- We release a dataset that contains the multimodal responses of four trajectory mining tasks on seven latest MLLM backbones. This dataset can shed light on future trajectory data mining research, such as fine-tuning a new MLLM specially used for trajectory data.

2 Related Works

Trajectory Data Mining. Existing research in trajectory data mining can be broadly divided into three categories. Early approaches focus on task-specific models designed for solving one specific task, such as travel time estimation [10, 31, 34, 47], trajectory prediction [6, 47], anomaly detection [9, 23, 29], or classification [3, 11, 19]. These works embed assumptions in model design, limiting their generalization ability for other tasks. To address this, trajectory foundation models [10, 18, 33–36, 39, 42, 45] are proposed to learn a unified model for various tasks. However, large-scale trajectories are required to pretrain these foundation models, leading to suboptimal performance on trajectories of unseen regions. Witnessing the progress of LLMs, several works try to solve the generalization problem with LLMs. These works treat LLMs as encoders [30, 37, 47],

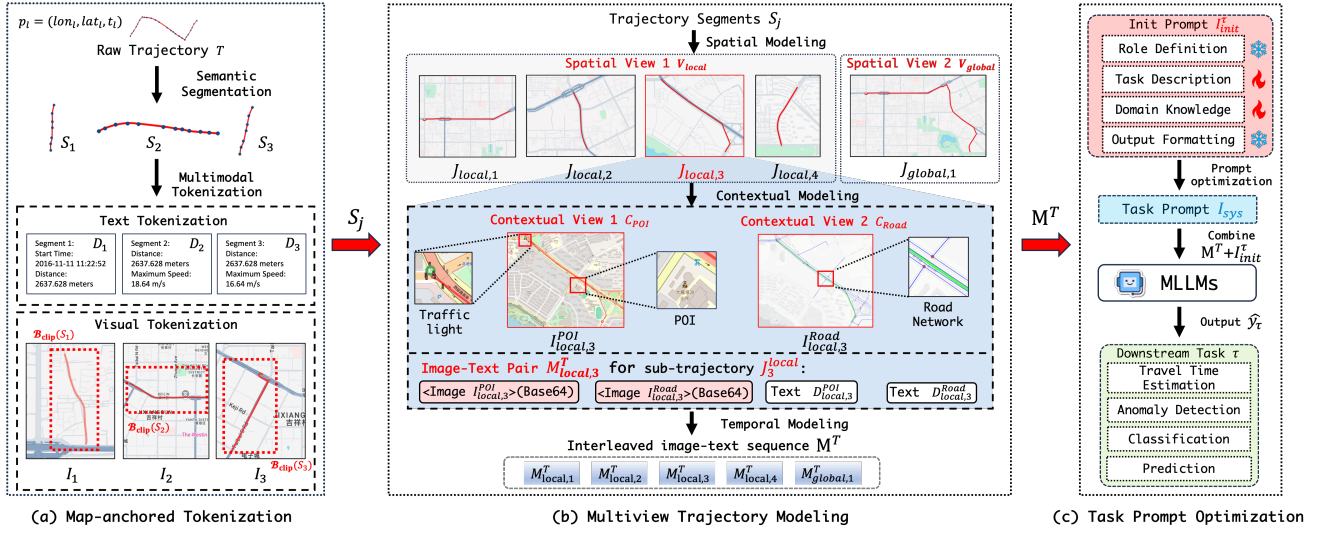


Figure 2: Overview of Traj-MLLM. Instead of direct model training, Traj-MLLM transforms raw trajectories into interleaved image-text sequences through map-anchored tokenization and multiview trajectory modeling. This enables us to reframe downstream tasks as multimodal reasoning problems, which can be directly solved by MLLMs in a training-free manner.

enhancer [41] and agents [5] to boost trajectory data mining. Nevertheless, the used LLMs are language models failing to handle image data, which is suitable for modeling the spatial and contextual information of trajectory. These researches inspire us to propose Traj-MLLM which is the first general framework utilizing MLLMs for trajectory data mining.

Multimodal Large Language Models. MLLMs have become a hot topic of recent AI research. Numerous works are proposed to either align visual modality to text[14, 15, 25] or enhance the multimodal reasoning ability[4, 12, 43]. The recent advances of MLLMs raise many geographical applications[13, 16, 28, 32, 40]. For example, MLLMs are now capable of inferring the geographic location of images, such as those shared on social media or captured from street views, based solely on visual content.[16, 28] However, most of current works are designed for analyzing static images, e.g. remote sensing pictures. Trajectory contains rich spatial-temporal and contextual information. Thus, current works cannot be directly used for trajectory data mining.

3 Preliminaries

In this section, we first define the problem of MLLM-based trajectory data mining, followed by a brief overview of Traj-MLLM.

Problem Definition: Assuming that a raw trajectory T consists of a sequence of points, $T = \{p_1, \dots, p_l, \dots, p_L\}$, where each point p_l consists of a GPS coordinate pair and a timestamp, i.e., (lon_l, lat_l, t_l) . Trajectory data mining tasks are denoted as a set \mathcal{T} , where $\tau \in \mathcal{T}$ is one specific task, such as travel time estimation, anomaly detection, or trajectory prediction. The problem of MLLMs-based trajectory data mining can be formally defined as follows:

Taking raw trajectory T and a task τ as inputs, there is a multimodal mapping function \mathcal{M} that first transforms T into visual and text modalities, denoted as I^T and D^T , and combines them to obtain the interleaved image-text sequence M^T . There is another prompt

construction function \mathcal{P} that generates the task prompt P^τ for task τ . Note that \mathcal{M} and \mathcal{P} are independent of each other, which makes the problem general for different geographical regions and tasks. The goal of MLLMs-based trajectory data mining is to generate the analysis result $\hat{y}_\tau = \text{MLLM}(M^T, P^\tau)$.

Overview of Traj-MLLM: As illustrated in Figure 2, Traj-MLLM consists of three key modules, i.e., map-anchored tokenization, multiview trajectory modeling, and task prompt optimization. The first two modules are designed to build the multimodal mapping function \mathcal{M} , and the third module is proposed for \mathcal{P} . To bridge the modality gap of trajectory data, raw trajectory T is segmented into sub-trajectories by map-anchored tokenization which encourages records having complete semantic information in one sub-trajectory. To model all the information required for different tasks, spatial, contextual, and temporal views of these sub-trajectories are constructed in the multiview trajectory modeling module to obtain an interleaved image-text sequence M^T of T . Finally, the task prompt optimization module is designed to obtain \mathcal{P} and achieve flexible task adaptation.

4 Methodology

In this section, we elaborate the three key modules in Traj-MLLM, i.e., map-anchored tokenization, multiview trajectory modeling and task prompt optimization in Section 4.1, 4.2 and 4.3, respectively. As the whole method is formulated for one trajectory, we omit the subscript T in the notations of following sections.

4.1 Map-Anchored Tokenization

Raw trajectory data consists of numerical coordinates and timestamps, lacking clear semantic structure, which makes it difficult to understand by MLLMs directly. Therefore, this module decomposes trajectories into semantic coherent sub-trajectories, and transform them into visual and text tokens.

4.1.1 Semantic Segmentation. A trajectory may contain semantically distinct phases, such as high-speed driving on highways, low-speed urban navigation, or stationary periods at intersections. Instead of feeding raw trajectory, sub-trajectories with coherent semantics can better capture fine-grained details and unleash the reasoning power of MLLMs. Therefore, Traj-MLLM conducts semantic segmentation at first and formulate it as an optimization problem.

Given a raw trajectory T , semantic segmentation aims to find a globally optimal segmentation $S = \{S_1, \dots, S_n, \dots, S_N\}$ by minimizing the sum of segment costs. We first project T on the map and define a cost function $\text{cost}(a, b)$ containing E map-anchored factors to quantify the semantic consistency of sub-trajectory from p_a to p_b :

$$\text{cost}(a, b) = \sum_{e=1}^E f_e(a, b) \quad (1)$$

In this paper, we utilize three factors, i.e. f_{speed} , f_{road} and f_{len} that capture motion, routing, and structural properties respectively. $f_{\text{speed}}(a, b)$ measures speed consistency that encourages sub-trajectory with stable motion, such as cruising at a constant speed or being stationary. $f_{\text{road}}(a, b)$ represents the number of road type changes, which prevents a sub-trajectory having different road types. $f_{\text{len}}(a, b)$ is a length regularization term that penalizes breaking the trajectory into too many short sub-trajectories. More details can be found in Appendix A.1.

To solve the optimization problem, we employ dynamic programming. Let $\text{DP}[h]$ denote the minimum cumulative cost for an optimal segmentation of the prefix trajectory $\{p_1, \dots, p_h\}$. The recurrence relation is defined by:

$$\text{DP}[h] = \min_{1 \leq d < h} (\text{DP}[d] + \text{cost}(d + 1, h)) \quad (2)$$

Here, h denotes the current endpoint of the subtrajectory for which the segmentation cost is being computed, and d indicates the candidate previous segmentation point. By computing $\text{DP}[h]$, we obtain the globally minimal cost for the entire trajectory. Then, by backtracking the DP table, the specific segment boundary $\{S_1, \dots, S_N\}$ that produces the optimal cost can be recovered. This approach effectively balances computational efficiency and segmentation quality, making it suitable for large-scale trajectory data analysis.

4.1.2 Multimodal Tokenization. After segmenting the trajectory into sub-trajectories, we convert each sub-trajectory $S_n \in S$ into multimodal tokens suitable for MLLM inference. Specifically, we generate two complementary representations: structured text tokens (D_n) that summarizes meta features and basic statistics; map-projected visual tokens (I_n) that combine spatial and contextual information. Here, we only provide a general method to generate these tokens. More details to obtain the interleaved image-text sequence of T are specified in Section 4.2.

Text Tokenization. For each sub-trajectory S_n , multiple statistical features are extracted from raw trajectory to generate a structured text description D_n .

$$D_n = \text{Concat}(\text{Time}(S_n), \text{Dist}(S_n), \text{Speed}(S_n), \dots) \quad (3)$$

The components here include $\text{Time}(\cdot)$ for the start and end timestamps, $\text{Dist}(\cdot)$ for the total distance traveled, and $\text{Speed}(\cdot)$ for summarizing dynamic metrics such as average speed and maximum

speed. These features are formatted to structured natural language sentences, providing semantic descriptions of S_n . More details can be found in Appendix A.2.

Visual Tokenization. To complement the text tokens, we generate visual tokens I_n which is the map-projected image. The image generation process contains three steps:

- (1) *Trajectory Rendering*: Each sub-trajectory S_n is rendered as a visually distinct polyline on a map tile service (e.g., OpenStreetMap). The start and end points of the segment are marked with unique icons to indicate direction.
- (2) *Map Clipping*: To focus the image on the relevant map area while preserving surrounding context, we dynamically calculate a minimal bounding box that encompasses all points within S_n . This bounding box is then expanded by a predefined padding factor Δ to obtain the clipping area.
- (3) *Image Capturing*: Leveraging a headless browser engine (e.g., Puppeteer), we capture a screenshot of the rendered map within the computed clipping area $\mathcal{B}_{\text{clip}}(S_n)$.

Note that the method above is a general version to clarify the basic idea of multimodal tokenization. Next, we will detail how to integrate spatial, contextual, and temporal information with the tokenization method.

4.2 Multiview Trajectory Modeling

After trajectory tokenization, a core challenge remains: how to uniformly integrate sufficient information for meeting the diverse demands of tasks and model the trajectory in a unified way. Given a sequence of sub-trajectories $S = \{S_1, \dots, S_n, \dots, S_N\}$ of trajectory T , multiview trajectory modeling aims to construct a multi-view interleaved image-text sequence M^T which contains different views of spatial scales $V = \{V_1, \dots, V_k, \dots, V_K\}$ and contextual information $C = \{C_1, \dots, C_z, \dots, C_K\}$.

Algorithm 1 Multiview Trajectory Modeling

Input: A sequence of sub-trajectories of a trajectory T , denoted as $S = \{S_1, \dots, S_n, \dots, S_N\}$.

Output: Multiview interleaved image-text sequence M^T .

```

1:  $M^T \leftarrow []$ 
2:  $V = \{V_1, \dots, V_K\} \leftarrow \text{GenerateSpatialViews}(S, \mathcal{G})$ 
3:  $C = \{C_1, \dots, C_K\} \leftarrow \text{GenerateContextualViews}()$ 
4: for each spatial view  $V_k \in V$  do
5:   for each sub-trajectory  $J_{k,i} \in J_k$  do
6:     for each contextual view  $C_z \in C$  do
7:        $I_{k,i}^z \leftarrow \text{GenerateVisual}(J_{k,i}, C_z)$  {Using the context information provided by  $C_j$ , generate image based on view  $J_{k,i}$ }
8:        $D_{k,i}^z \leftarrow \text{GenerateText}(J_{k,i}, C_z)$  {Generate statistical text description for  $J_{k,i}$ }
9:        $M^T.append((I_{k,i}^z, D_{k,i}^z))$ 
10:    end for
11:  end for
12: end for
13: return  $M^T$ 
```

4.2.1 Spatial Information Modeling. To model coarse-to-fine spatial information of T , a set of K spatial views, $V = \{V_1, \dots, V_k, \dots, V_K\}$

is constructed to describe the trajectory at different scales. Each spatial view V_k represents a scale of trajectory T and can be obtained by combining sub-trajectories with a specific coarse-grained strategy g_k . For trajectory T , we construct a set of coarse-grained strategies $\mathcal{G} = \{g_1, \dots, g_k, \dots, g_K\}$ which convert multimodal representations for different spatial scales.

Formally, by applying g_k on the sub-trajectories S , we can obtain a partition of S , denote as $J_k = \{J_{k,1}, \dots, J_{k,i}, \dots, J_{k,I}\}$, where $J_{k,i}$ is a combination of successive sub-trajectories, e.g., $J_{k,1} = \{S_1, S_2, \dots\}$ and $J_{k,i} = \{S_{n-1}, S_n, \dots\}$. As illustrated in Figure 2(b), we construct two coarse-grained strategies, i.e., g_{global} and g_{local} . g_{global} takes T as a whole to generate the global view V_{global} , and g_{local} treats each sub-trajectory independently to generate the local view V_{local} . Notice that T contains four sub-trajectories, the spatial information modeling of T can be formalized as follows: $V_{local} = \{J_{local,1}, J_{local,2}, J_{local,3}, J_{local,4}\}$, and $V_{global} = J_{global,1}$.

To obtain multimodal representation, each $J_{k,i}$ can also be viewed as a sub-trajectory of T . We can get the structured text tokens $D_{k,i}$ and visual tokens $I_{k,i}$ for each sub-trajectory $J_{k,i}$ by applying the **Map-Anchored Tokenization** module described in Section 4.1. The combination of multimodal representations of these spatial views captures the coarse-to-fine spatial semantics of the trajectory.

4.2.2 Contextual Information Modeling. Traj-MLLM enriches the visual tokens of spatial view partitions to integrate various contextual information. We introduce a set of contextual views $C = \{C_1, \dots, C_z, \dots, C_Z\}$, each representing a different type of contextual information relevant to the trajectory, such as POIs, road networks, and traffic lights. Given an arbitrary $J_{k,i} \in J_k$, we extend the visual tokenization method described in Section 4.1.2 and generate image $\{I_{k,i}^z\}_{z \in 1 \dots Z}$ for each context view $C_z \in C$.

As illustrated in Figure 2(b), we enrich the spatial views by POIs and road networks, and obtain $I_{k,i}^{POI}$ and $I_{k,i}^{road}$. We employ two key strategies to ensure the resulting images are informative yet clear. **Layer Decomposition.** Directly overlaying all available contextual data on a single image would obscure the useful information in visual clutter. To address this, we decompose contextual information into distinct visual map layers. Each map layer can be treated as a contextual view of T . Thus, the map layer decomposition produces multiple contextual views for a single spatial $J_{k,i}$. As shown, $I_{k,i}^{POI}$ and $I_{k,i}^{road}$ are generated for T .

Context Filtering. However, due to the large amount of contextual data available in a region, it is necessary to filter the most relevant information for the trajectory. Specifically, we filter the context elements rendered in each view based on their relevance to the sub-trajectory $J_{k,i}$. Let $\mathcal{E}_{k,i}^z$ denote the full set of context elements associated with view type C_z . We define a general scoring function $\text{dis}(e, J_{k,i})$ that measures how closely a context element $e \in \mathcal{E}_{k,i}^z$ relates to the sub-trajectory represented in $J_{k,i}$. We retain only those elements below a threshold θ which represents the relevance of the trajectory:

$$\mathcal{E}_{k,i}^{z*} = \{e \in \mathcal{E}_{k,i}^z \mid \text{dis}(e, J_{k,i}) \leq \theta\} \quad (4)$$

In practice, we realize the relevance function primarily based on spatial proximity. For example, in a POI-centric view, the element set $\mathcal{E}_{k,i}^{POI}$ consists of all POIs in the region. The filtered subset is

defined as:

$$\mathcal{E}_{k,i}^{POI*} = \{e \in \mathcal{E}_{k,i}^{POI} \mid \text{dis}^{POI}(e, J_{k,i}) \leq \theta_{POI}\}, \quad (5)$$

where $\text{dis}^{POI}(e, J_{k,i})$ is the shortest Euclidean distance from the POI e to $J_{k,i}$ and the θ_{POI} is the distance threshold.

Furthermore, to visually highlight the trajectories, we present them clearly enough to distinguish trajectories from the contextual data. As shown in Figure 2, we use thick red lines in the POI-centric view or thick green lines in the road network view. These vision and filtering strategies can effectively guide MLLMs to understand critical contextual cues.

4.2.3 Temporal Information Modeling. Temporal order is a fundamental property of trajectories. Instead of using a trainable temporal encoder, Traj-MLLM exploits the sequential modeling capability of MLLMs to capture the temporal information. By arranging the multimodal tokens of all generated spatial and contextual views, we can obtain an interleaved image-text sequence for T .

Formally, given a set of multimodal tuples $\{(I_{k,i}^z, D_{k,i}^z)\}$ where $k \in (1, K)$, $i \in [1, I]$ and $z \in [1, Z]$, we assemble them into an ordered interleaved image-text sequence $M^T = [M_1^T, \dots, M_k^T, \dots, M_K^T]$ to capture temporal dependencies. Each M_k^T corresponds to a spatial view V_k . Each M_k^T is further composed of I spatial sub-views, denoted as $M_k^T = [M_{k,1}^T, \dots, M_{k,i}^T, \dots, M_{k,I}^T]$. Each sub-view $M_{k,i}^T$ consists of Z multimodal pairs derived from different contextual views $C = \{C_1, \dots, C_z, \dots, C_Z\}$. The overall process is summarized in Algorithm 1.

$$M_{k,i}^T = [(I_{k,i}^1, D_{k,i}^1), \dots, (I_{k,i}^z, D_{k,i}^z)], \quad (6)$$

where $(I_{k,i}^z, D_{k,i}^z)$ denotes the image-text pair in contextual view C_z .

As shown in Figure 2(b), the sequence $M_{local,3}^T$ refers to the third sub-trajectory $J_{local,3}$ of the local spatial view V_{local} . It contains multimodal pairs from two contextual views: the POI-centric view C_{POI} and the road network view C_{road} , denoted as $(I_{local,3}^{POI}, D_{local,3}^{POI})$ and $(I_{local,3}^{road}, D_{local,3}^{road})$, respectively.

The images are encoded as base64 to fit the inputs of MLLM prompt. The corresponding text description both provides a semantic interpretation of the image and serves as a text anchor (e.g., "POI image of segment 1: <image>"). This structured and sequential presentation enables MLLMs to naturally interpret trajectories as temporally coherent narratives, effectively capturing time-dependent relationships without additional training.

4.3 Task Prompt Optimization

To achieve flexible task adaptation, we propose to model the task-specified information in the task prompt instead of training task heads. However, both the reasoning steps and used information of different tasks vary significantly. It is challenging to construct a data-invariant task prompt that can be easily understood by MLLMs and suitable for different trajectories. This module aims to address this challenge with a few labeled seed trajectories (e.g., less than 10) and conducts multi-rounds interaction with MLLMs to optimize the task prompts. Next, we first introduce the construction of task prompt template, and then describe the optimization process.

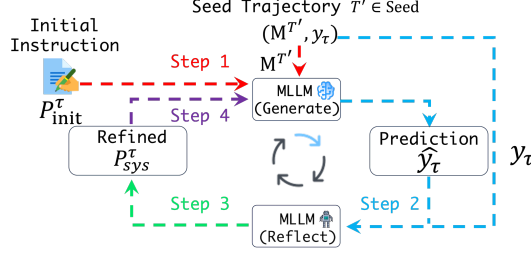


Figure 3: Task Prompt Optimization.

4.3.1 Task Prompt Template. For each trajectory mining task τ , we generate the task prompt with a general prompt template. The task prompt P_{sys} consists of four components:

$$P_{\text{sys}} = (P_{\text{role}}, P_{\text{task}}, P_{\text{know}}, P_{\text{format}}) \quad (7)$$

Here, the Role Definition (P_{role}) and Output Format (P_{format}) are fixed for each task. The optimization focuses on refining the Task Description (P_{task}) and Domain Knowledge (P_{know}).

4.3.2 Prompt Optimization. In this module, Traj-MLLM takes an initial prompt P_{init}^{τ} predefined by human experience and a few seed trajectories as inputs. We aim to optimize P_{init}^{τ} into a more effective prompt P_{sys}^{τ} through an automated, MLLM refinement loop. As shown in Figure 3, the optimization proceeds as follows: (1) We first select a set of seed trajectories Seed and generate their corresponding interleaved image-text sequence set $\mathbb{M} = \{\mathbf{M}^{T'} \mid T' \in \text{Seed}\}$; (2) For each $T' \in \text{Seed}$, we feed its interleaved image-text sequence $\mathbf{M}^{T'}$ and the initial system prompt P_{init}^{τ} into the MLLM to obtain the output y ; (3) We construct a feedback loop, i.e., MLLM reflects on its output y in light of the true label \hat{y} , generating suggestions to improve the prompt. Based on the feedback from disagreement samples, the MLLM generates a refined prompt P_{sys}^{τ} , which is subsequently used to re-evaluate other seed trajectories; (4) Repeat (2)-(3) several times, allowing MLLM to self-improve the prompt based on feedback. The process concludes when the refined prompt P_{sys}^{τ} demonstrates satisfactory performance on Seed .

Notice that once P_{sys}^{τ} is finalized, it can be directly reused across different regions by simply updating some location-specific parts in P_{know} , such as the population and city scale.

Model Inference. Once P_{sys}^{τ} is finalized, inferring any new trajectory T is straightforward. The trajectory is first transformed into an interleaved image-text sequence \mathbf{M}^T (see Sections 4.1 and 4.2). This sequence, together with the optimized prompt P_{sys}^{τ} , is used as input to the MLLM, which generates a textual response. The output is then parsed according to P_{format} to extract structured results.

5 Experiment

We conduct experiments to answer the following questions:

- RQ1:** How does Traj-MLLM perform on different tasks?
- RQ2:** How does Traj-MLLM perform on different MLLM backbones?
- RQ3:** What is the efficiency of Traj-MLLM?
- RQ4:** What are the influences of the proposed components?
- RQ5:** How is the reasoning ability of Traj-MLLM?
- RQ6:** What are the influences of hyper-parameter θ ?

5.1 Experimental Settings

In this section, we briefly introduce the datasets, tasks, evaluation metrics, and baselines. All the datasets and codes of Traj-MLLM are released¹. More detailed settings can be found in Appendix A.3.

Datasets. We conduct extensive experiments on four public trajectory datasets, Xian, Chengdu², Porto³ and Geolife[44]. The map layers, road networks and POIs are obtained by OpenStreetMap⁴. Due to budget constraints, we select over 80,000 trajectories and perform four tasks to obtain about 320,000 MLLMs responses.

Tasks and Evaluation Metrics. We choose four tasks that are widely studied in trajectory data mining, i.e., travel time estimation (TTE) [31, 45], anomaly detection (AD) [26, 29], mobility prediction (MP) [47] and transportation mode identification (TMI) [46], to evaluate the effectiveness of Traj-MLLM. We follow existing works[29, 31, 46] to choose the same metrics. For TTE, we report mean absolute error (MAE), root mean squared error (RMSE), and mean absolute percentage error (MAPE). For AD, we evaluate the performance with precision-recall area under the curve (PR-AUC). For MP, we choose Top-1 Accuracy (ACC@1) and Top-5 Accuracy (ACC@5). For TMI, we report Accuracy, Macro-F1, and Weighted-F1. More details can be found in Appendix A.3.2.

Baselines. For each task, we choose three kinds of baselines, i.e., task-specified models, trajectory foundation models and LLM-based models. The baselines for TTE and MP include Traj2Vec [36], T2Vec [18], Trember [7], CTLE [22], Toast [2], TrajCL [1], MMTEC [21], JGRM [24], START [10], UniTR[42], BigCity[37] and BLUE[45], PLM4Traj [47] and Path-LLM[30] and MM-Path [31]. For AD, we compare Traj-MLLM against iBAT [38], GM-VSAE [23], ATROM [8], DeepTEA [9], MST-OATD [29], and FOTraj [26]. For TMI, Traj-MLLM is compared with SECA [3], TrajODE [20], TrajFormer [19], and RED [46].

5.2 Effectiveness of Traj-MLLM (RQ1)

To answer **RQ1**, we compare Traj-MLLM against multiple baselines across four tasks on four datasets. The results show that Traj-MLLM consistently achieves the best performance on all tasks and regions. Notice that Traj-MLLM achieves these results without any training or fine-tuning.

For TTE, we report the results in Table 1 and derive three observations. (1) Traj-MLLM outperforms all baselines across all three datasets. For instance, compared to the strongest multimodal baseline MM-Path, Traj-MLLM reduces the MAE by over 29% on Xian, 15% on Porto, and 21% on Chengdu. This consistent improvement demonstrates the effectiveness of Traj-MLLM. (2) Although MM-Path considers the image modality, it is also inferior to Traj-MLLM because multiview trajectory modeling provides richer contextual information to inspire the reasoning ability of MLLMs. (3) Traj-MLLM achieves over 34.9% performance improvements on MAPE compared to the LLM-based methods, i.e. PLM4Traj and Path-LLM. This result demonstrates that Traj-MLLM performs better than fine-tuning a small LLM, e.g., GPT-2.

The results of MP are summarized in Table 1. MP requires capturing fine-grained spatial-temporal information of the trajectory. Similar to TTE, we observe over 15% improvements of ACC@1

¹<https://anonymous.4open.science/r/Traj-MLLM/>

²<https://outreach.didichuxing.com/>

³<https://www.kaggle.com/c/pkdd-15-predict-taxi-service-trajectory>

⁴<https://www.openstreetmap.org/>

Table 1: Performance on Travel Time Estimation and Mobility Prediction.

Methods	Xian					Porto					Chengdu				
	Travel Time Est.			Mobility Pred.		Travel Time Est.			Mobility Pred.		Travel Time Est.			Mobility Pred.	
	MAE	RMSE	MAPE	ACC@1	ACC@5	MAE	RMSE	MAPE	ACC@1	ACC@5	MAE	RMSE	MAPE	ACC@1	ACC@5
Traj2Vec[36]	230.98	382.31	28.18	42.31	72.99	210.12	362.76	26.61	43.77	73.98	238.92	390.11	29.11	42.12	71.88
T2Vec[18]	228.84	377.63	27.28	43.21	74.01	208.22	355.47	26.23	44.22	75.27	234.52	378.24	28.87	44.01	73.23
Trember[7]	223.73	377.23	25.82	49.72	79.17	204.49	347.66	24.56	49.57	79.82	231.55	377.15	25.92	49.72	79.54
CTLE[22]	232.29	377.34	26.82	50.83	80.14	205.53	355.82	26.25	50.22	80.65	228.52	388.31	25.88	50.23	81.02
Toast[2]	226.65	378.92	26.18	50.57	80.07	204.24	353.43	26.11	50.09	80.21	228.12	386.78	25.81	49.97	80.22
TrajCL[1]	218.12	365.12	25.44	49.81	79.92	198.23	340.44	24.11	49.96	79.81	222.13	368.33	25.65	49.82	79.87
START[10]	203.11	339.90	24.01	49.71	80.29	195.49	354.22	23.84	51.98	81.37	196.44	314.14	24.12	53.22	86.47
MMTEC[21]	201.23	332.18	23.91	52.25	81.16	194.21	352.34	23.67	51.99	81.13	195.32	318.98	24.02	53.12	86.52
UniTR[42]	204.93	345.33	25.14	51.67	79.39	199.41	347.59	23.82	50.11	80.14	208.44	339.23	24.82	52.87	84.10
JGRM[24]	202.19	332.88	23.98	52.28	81.02	194.43	352.45	23.78	52.01	81.29	195.34	314.62	24.01	53.11	86.42
BLUE[45]	186.34	298.13	19.35	49.45	80.44	171.22	298.11	19.32	48.43	81.72	169.22	264.93	20.11	57.90	83.24
MM-Path[31]	197.41	317.85	22.85	48.76	81.67	181.16	320.66	22.12	48.16	80.92	187.03	279.40	22.76	58.88	84.17
BigCity[37]	198.78	325.98	23.69	50.12	80.33	186.91	329.39	22.72	51.44	81.01	188.42	301.11	23.18	55.23	81.76
PLM4Traj[47]	196.72	334.42	23.61	52.76	82.15	189.99	344.64	22.89	52.33	81.44	189.09	298.24	23.21	59.50	86.27
Path-LLM[30]	192.76	313.88	23.54	50.85	80.73	184.42	323.83	22.67	50.15	80.87	184.67	294.55	22.97	56.44	82.45
Traj-MLLM	131.02	154.86	15.36	60.72	83.25	144.63	173.54	15.14	60.45	82.33	133.43	154.67	16.34	60.12	87.22
<i>Improvement</i>	29.69%	48.05%	20.62%	15.09%	1.34%	15.53%	41.79%	21.64%	15.52%	0.75%	21.15%	41.62%	18.75%	1.04%	0.81%

Table 2: Performance on Anomaly Detection (PR-AUC score).

Method	Xian					Porto					Chengdu				
	Detour			Switch		Detour			Switch		Detour			Switch	
	Low	Medium	High	$\mu = 0.3$	$\mu = 0.5$	Low	Medium	High	$\mu = 0.3$	$\mu = 0.5$	Low	Medium	High	$\mu = 0.3$	$\mu = 0.5$
iBAT[38]	0.439	0.487	0.694	0.199	0.262	0.273	0.313	0.501	0.201	0.241	0.450	0.497	0.691	0.201	0.254
GM-VSAE[23]	0.854	0.921	0.944	0.521	0.612	0.374	0.722	0.910	0.871	0.893	0.858	0.919	0.947	0.547	0.609
ATROM[8]	0.816	0.897	0.901	0.532	0.601	0.386	0.709	0.882	0.845	0.881	0.841	0.872	0.921	0.535	0.611
DeepTEA[9]	0.871	0.932	0.940	0.576	0.654	0.408	0.736	0.921	0.861	0.872	0.875	0.931	0.935	0.576	0.655
MST-OATD[29]	0.902	0.951	0.971	0.598	0.691	0.739	0.892	0.970	0.899	0.912	0.907	0.949	0.969	0.604	0.677
FOTraj[26]	0.911	0.954	0.979	0.625	0.733	0.741	0.901	0.974	0.927	0.946	0.913	0.954	0.971	0.649	0.656
Traj-MLLM	0.967	0.979	0.981	0.947	0.956	0.968	0.980	0.981	0.971	0.981	0.967	0.976	0.980	0.966	0.983
<i>Improvement</i>	6.15%	2.62%	0.20%	51.52%	30.42%	30.63%	8.77%	0.72%	4.75%	3.70%	5.91%	2.31%	0.93%	48.84%	45.19%

Table 3: Performance on Transportation Mode Identification.

Method	Geolife		
	Accuracy	Macro-F1	Weighted-F1
SECA[3]	78.91	78.78	79.02
TrajODE[20]	85.48	84.98	85.17
TrajFormer[19]	85.56	85.12	85.71
RED[46]	85.89	85.23	86.11
Traj-MLLM	87.46	86.71	87.45
<i>Improvement</i>	1.83%	1.74%	1.56%

on Xian and Porto compared to the strongest baseline PLM4Traj, demonstrating that Traj-MLLM can guide MLLMs to understand complex and fine-grained mobility patterns.

The results of anomaly detection are presented in Table 2. From these results, we observe: (1) Traj-MLLM achieves the best performance among all baselines, consistently outperforming on all datasets, anomaly types, and perturbation levels. (2) Traj-MLLM is robust on both subtle detour and complex switch anomalies, maintaining stable performance under varying perturbation magnitudes. For instance, the PR-AUC score increases from 0.741 to 0.968 for low-magnitude detour anomalies. This improvement can be attributed to the *multiview trajectory modeling*, which provides multi-scale spatial information that encourages the model to capture diverse anomalous patterns. (3) Traj-MLLM achieves high performance without requiring any model training or explicit anomaly examples, enabling to generalize Traj-MLLM to unseen regions.

Moreover, we present the transportation mode identification results in Table 3. As illustrated, Traj-MLLM improves accuracy

by 1.83% over RED[46]. By feeding multimodal information to the MLLM, Traj-MLLM is able to combine visual cues from the map (e.g., the presence of railway tracks) and statistical information from the text prompts (e.g., velocity and acceleration) to infer the transportation mode. In summary, across the four tasks, Traj-MLLM can leverage the MLLM’s capacity for both fine-grained spatial analysis (as in TTE and MP) and high-level semantic reasoning (as in AD and TMI). according to these results, we argue that Traj-MLLM has strong generalization ability to achieve region-agnostic and task-adaptive trajectory data mining without the requirement of any data.

5.3 Performance of different MLLMs (RQ2)

To answer RQ2, we explore the performance of Traj-MLLM under seven MLLM backbones on the Porto dataset across two tasks, *i.e.* TTE and AD (detour anomalies). The results are shown in Figure 4. According to the results, we have three observations: (1) Within the same model family, closed-source models tend to outperform open-source models. For example, the closed-source qwen-vl-max achieves better results on both tasks than the open-source model qwen-2.5-vl-72b, which may be due to its architecture or proprietary optimizations during training. (2) Model scale is not the sole determinant of performance. Notably, the open-source gemma-3-27b-it performs better than the larger qwen-2.5-vl-72b and achieves a PR-AUC score nearly on par with the powerful closed-source gemini-2.5-pro. This highlights the significant potential and bright

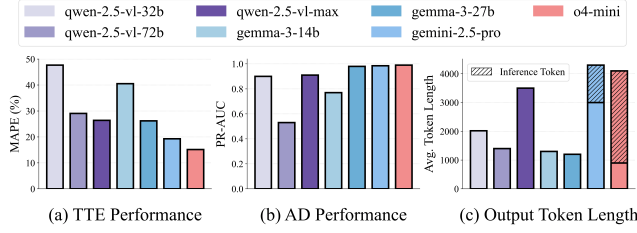


Figure 4: Performance with different MLLMs.

Table 4: Efficiency of Different MLLMs.

Model	Latency	Throughput	AvgTime	Cost
gemma-3-14b	14.1	178.6	0.079	\$0.002
gemma-3-27b	11.2	268.1	0.042	\$0.004
qwen2.5-vl-32b	15.2	189.9	0.080	\$0.006
qwen-vl-max	10.4	277.3	0.038	\$0.017
qwen2.5-vl-72b	19.3	149.2	0.129	\$0.018
gemini-2.5-pro	32.0	89.9	0.356	\$0.024
o4-mini	9.23	312.5	0.030	\$0.014

future of open-source models in trajectory data mining. (3) As shown in Figure 4(c), o4-mini achieves the best results on both tasks while generating the shortest output responses. Its superior performance and efficiency can be attributed to its longest inference tokens. Given its dominant performance, we select o4-mini as the default MLLM backbone to report our performances. We show the output differences of different MLLMs in Appendix A.5.2

5.4 Efficiency of Traj-MLLM (RQ3)

To answer RQ3, we evaluate the efficiency of Traj-MLLM by measuring inference latency, throughput, average time, and cost on different MLLM backbones. The throughput and average time are calculated based on the maximum allowed for the API provider’s highest access tier (e.g., o4-mini has a throughput of 150M tokens per minute (TPM)). The results are summarized in Table 4.

As shown in the table, we have the following observations: (1) o4-mini is the most efficient, achieving the lowest latency and the highest throughput. In contrast, gemini-2.5-pro is the slowest model due to its significantly longer response time. (2) In terms of cost, gemma-3-14b is the most economical choice, which can be attributed to its smaller parameter size. The gemini-2.5-pro is the most expensive model owing to its large number of output tokens. (3) With the large scale deployment of MLLMs, the throughput increases and average processing time of each trajectory drops sharply, *i.e.*, 0.030s per trajectory. These results highlight the trade-offs between inference speed, throughput, and cost to use MLLMs.

Table 5: Ablation Study Results on the Chengdu Dataset.

Method	Chengdu				
	Travel Time Estimation			Anomaly Detection	
	MAE ↓	RMSE ↓	MAPE ↓	F1-score ↑	PR-AUC ↑
w/o image	350.15	392.33	35.97	-	-
w/o seg	243.26	357.02	28.44	0.788	0.821
w/o order	330.23	368.12	32.87	0.952	0.953
w/o POI	194.06	247.79	19.92	0.940	0.942
w/o road	234.91	304.88	24.75	0.862	0.871
Traj-MLLM	133.43	154.67	16.34	0.980	0.980

5.5 Ablation Study (RQ4)

We compare Traj-MLLM with five ablations on two downstream tasks to analyze the effectiveness of the proposed components. We obtain **w/o image**, **w/o segment**, **w/o order**, **w/o POI**, and **w/o road**, by removing the visual modality, replacing the principled segmentation with a naive strategy, breaking the correspondence between textual descriptions and their visual components, removing the POI-centric view, and removing the road-network-centric view, respectively. The results are summarized in Table 5.

Removing the image modality (**w/o image**) causes the most significant performance drop on both tasks. This indicates that constructing visual representations is crucial for MLLMs to understand trajectory details. Breaking the order of visual-text pairs (**w/o order**), which removes temporal correspondence, also leads to a notable performance decrease. This means that temporal order is crucial to capture trajectory dynamics accurately. Replacing our semantic segmentation approach with a naive segmentation strategy (**w/o segment**) also leads to large performance degradation, demonstrating that the local detail view obtained through semantically coherent segmentation can provide crucial information. Furthermore, the lack of POI-centric view and road network-centric view also significantly reduces the performance. In a word, these ablation results support that the designed components of Traj-MLLM have positive contributions to the performance of Traj-MLLM.

5.6 Reasoning Ability Analysis (RQ5)

To answer RQ5, we analyze the reasoning ability of Traj-MLLM. Due to the space limit, we show the case figures and more detailed analysis in Appendix A.5. Traj-MLLM demonstrates strong reasoning abilities in two key aspects: (1) For **interpretable result**, Traj-MLLM provides detailed, step-by-step reasoning. For example, in the anomaly detection task, it not only identifies an anomalous trajectory but also precisely locates the anomalous segments and explains its conclusion by referencing the multimodal information. (2) For **multi-round reasoning**, the model can adapt its predictions based on real-time contextual updates. For instance, in the TTE task, after being notified of traffic congestion on a specific road, Traj-MLLM incorporates this new information to revise its initial travel time estimation. These capabilities show that Traj-MLLM functions as an interactive reasoning engine, not just a static prediction model.

5.7 Sensitivity Analysis of θ (RQ6)

We conduct a sensitivity analysis on θ to investigate how different distance thresholds between context elements and the trajectory affect downstream task performance. According to the results presented in Figure 5, we have two key observations: (1) For all datasets, task performance consistently drops when the distance threshold exceeds 100m, indicating that larger thresholds introduce excessive irrelevant contextual information, which negatively impacts downstream tasks. (2) The optimal threshold differs by dataset: for Porto, the best results are achieved at 50m, while for Chengdu and Xian, 100m yields the highest performance. This difference reflects the variations in urban layouts—Chengdu and Xian have more regular road networks, making 100m a balanced choice between informativeness and noise. In contrast, Porto’s dense and irregular road

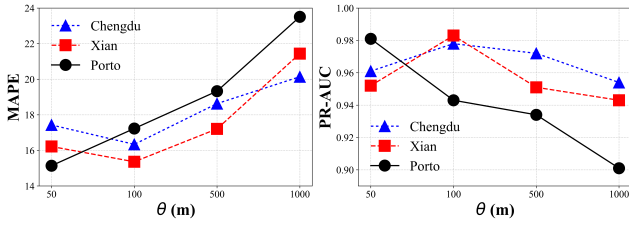


Figure 5: Sensitivity Analysis.

structure favors a smaller 50m threshold to avoid interference from unrelated elements. More details are in Appendix A.4.

6 Conclusion

In this paper, we propose a novel training-free framework Traj-MLLM which is the first work employing the reasoning ability of MLLMs for trajectory data mining. By effectively bridging the semantic gap of raw trajectory, Traj-MLLM integrates multiview contexts and transforms trajectories into multimodal sequences, enabling the use of the reasoning ability of MLLMs directly. Experiments on multiple representative tasks and cross-city datasets show that Traj-MLLM achieves performance improvements while maintaining strong generalization ability without any training or fine-tuning. We also release all the data responded by MLLMs, which can be used as the foundation for future research in training MLLMs specialized for trajectories and analyzing other spatial-temporal data.

References

- [1] Yanchuan Chang, Jianzhong Qi, Yuxuan Liang, and Egemen Tanin. 2023. Contrastive trajectory similarity learning with dual-feature attention. In *2023 IEEE 39th International conference on data engineering (ICDE)*. IEEE, 2933–2945.
- [2] Yile Chen, Xiucheng Li, Gao Cong, Zhifeng Bao, Cheng Long, Yiding Liu, Arun Kumar Chandran, and Richard Ellison. 2021. Robust road network representation learning: When traffic patterns meet traveling semantics. In *Proceedings of the 30th ACM International Conference on Information & Knowledge Management*. 211–220.
- [3] Sina Dabiri, Chang-Tien Lu, Kevin Heaslip, and Chandan K Reddy. 2019. Semi-supervised deep learning approach for transportation mode identification using GPS trajectory data. *IEEE Transactions on Knowledge and Data Engineering* 32, 5 (2019), 1010–1023.
- [4] Yuhao Dong, Zuyan Liu, Hai-Long Sun, Jingkan Yang, Winston Hu, Yongming Rao, and Ziwei Liu. 2025. Insight-v: Exploring long-chain visual reasoning with multimodal large language models. In *Proceedings of the Computer Vision and Pattern Recognition Conference*. 9062–9072.
- [5] Yuwei Du, Jie Feng, Jie Zhao, and Yong Li. 2024. Trajagent: An agent framework for unified trajectory modelling. *arXiv e-prints* (2024), arXiv:2410.2410.
- [6] Jie Feng, Yong Li, Chao Zhang, Funing Sun, Fanchao Meng, Ang Guo, and Depeng Jin. 2018. Deepmove: Predicting human mobility with attentional recurrent networks. In *Proceedings of the 2018 world wide web conference*. 1459–1468.
- [7] Tao-Yang Fu and Wang-Chien Lee. 2020. Trembr: Exploring road networks for trajectory representation learning. *ACM Transactions on Intelligent Systems and Technology (TIST)* 11, 1 (2020), 1–25.
- [8] Qiang Gao, Xiaohan Wang, Chaoran Liu, Goce Trajcevski, Li Huang, and Fan Zhou. 2023. Open anomalous trajectory recognition via probabilistic metric learning. In *IJCAI International Joint Conferences on Artificial Intelligence Organization*.
- [9] Xiaolin Han, Reynold Cheng, Chenhao Ma, and Tobias Grubenmann. 2022. DeepTEA: Effective and efficient online time-dependent trajectory outlier detection. *Proceedings of the VLDB Endowment* 15, 7 (2022), 1493–1505.
- [10] Jiawei Jiang, Dayan Pan, Houxing Ren, Xiaohan Jiang, Chao Li, and Jingyuan Wang. 2023. Self-supervised trajectory representation learning with temporal regularities and travel semantics. In *2023 IEEE 39th international conference on data engineering (ICDE)*. IEEE, 843–855.
- [11] Xiang Jiang, Erico N de Souza, Ahmad Pesaranghader, Baifan Hu, Daniel L Silver, and Stan Matwin. 2017. Trajectorynet: An embedded gps trajectory representation for point-based classification using recurrent neural networks. *arXiv preprint arXiv:1705.02636* (2017).
- [12] Jihyung Kil, Zheda Mai, Justin Lee, Arpita Chowdhury, Ziheng Wang, Kerrie Cheng, Lemeng Wang, Ye Liu, and Wei-Lun Harry Chao. 2024. Mllm-compench: A comparative reasoning benchmark for multimodal llms. *Advances in Neural Information Processing Systems* 37 (2024), 28798–28827.
- [13] Kartik Kuckreja, Muhammad Sohail Danish, Muzammal Naseer, Abhijit Das, Salman Khan, and Fahad Shahbaz Khan. 2024. GeoChat: Grounded large vision-language model for remote sensing. In *Proceedings of the IEEE/CVF Conference on Computer Vision and Pattern Recognition*. 27831–27840.
- [14] Junnan Li, Dongxu Li, Silvio Savarese, and Steven Hoi. 2023. Blip-2: Bootstrapping language-image pre-training with frozen image encoders and large language models. In *International conference on machine learning*. PMLR, 19730–19742.
- [15] Junnan Li, Dongxu Li, Caiming Xiong, and Steven Hoi. 2022. Blip: Bootstrapping language-image pre-training for unified vision-language understanding and generation. In *International conference on machine learning*. PMLR, 12888–12900.
- [16] Ling Li, Yu Ye, Bingchuan Jiang, and Wei Zeng. 2024. Georeasoner: Geolocalization with reasoning in street views using a large vision-language model. In *Forty-first International Conference on Machine Learning*.
- [17] Wenbin Li, Di Yao, Ruibo Zhao, Wenjie Chen, Zijie Xu, Chengxue Luo, Chang Gong, Quanliang Jing, Haining Tan, and Jingping Bi. 2025. Sbench: Assessing the ability of large language models in spatio-temporal analysis. In *Companion Proceedings of the ACM on Web Conference 2025*. 749–752.
- [18] Xiucheng Li, Kaiqi Zhao, Gao Cong, Christian S Jensen, and Wei Wei. 2018. Deep representation learning for trajectory similarity computation. In *2018 IEEE 34th international conference on data engineering (ICDE)*. IEEE, 617–628.
- [19] Yuxuan Liang, Kun Ouyang, Yiwei Wang, Xu Liu, Hongyang Chen, Junbo Zhang, Yu Zheng, and Roger Zimmermann. 2022. TrajFormer: Efficient trajectory classification with transformers. In *Proceedings of the 31st ACM International Conference on Information & Knowledge Management*. 1229–1237.
- [20] Yuxuan Liang, Kun Ouyang, Hanshu Yan, Yiwei Wang, Zekun Tong, and Roger Zimmermann. 2021. Modeling Trajectories with Neural Ordinary Differential Equations.. In *IJCAI*. 1498–1504.
- [21] Yan Lin, Huaiyu Wan, Shengnan Guo, Jilin Hu, Christian S Jensen, and Youfang Lin. 2023. Pre-training general trajectory embeddings with maximum multi-view entropy coding. *IEEE Transactions on Knowledge and Data Engineering* 36, 12 (2023), 9037–9050.
- [22] Yan Lin, Huaiyu Wan, Shengnan Guo, and Youfang Lin. 2021. Pre-training context and time aware location embeddings from spatial-temporal trajectories for user next location prediction. In *Proceedings of the AAAI conference on artificial intelligence*, Vol. 35. 4241–4248.
- [23] Yiding Liu, Kaiqi Zhao, Gao Cong, and Zhifeng Bao. 2020. Online anomalous trajectory detection with deep generative sequence modeling. In *2020 IEEE 36th International Conference on Data Engineering (ICDE)*. IEEE, 949–960.
- [24] Zhipeng Ma, Zheyang Tu, Xinhai Chen, Yan Zhang, Deguo Xia, Guyue Zhou, Yilun Chen, Yu Zheng, and Jiangtao Gong. 2024. More than routing: Joint GPS and route modeling for refine trajectory representation learning. In *Proceedings of the ACM Web Conference 2024*. 3064–3075.
- [25] Alec Radford, Jong Wook Kim, Chris Hallacy, Aditya Ramesh, Gabriel Goh, Sandhini Agarwal, Girish Sastry, Amanda Askell, Pamela Mishkin, Jack Clark, et al. 2021. Learning transferable visual models from natural language supervision. In *International conference on machine learning*. PMLR, 8748–8763.
- [26] Wei Shao, Ziquan Fang, Lu Chen, and Yunjun Gao. 2025. Towards Trajectory Anomaly Detection: A Fine-Grained and Noise-Resilient Framework. In *Proceedings of the 31st ACM SIGKDD Conference on Knowledge Discovery and Data Mining*.
- [27] Jiahui Sun, Haiming Jin, Zhaoxing Yang, Lu Su, and Xinbing Wang. 2022. Optimizing long-term efficiency and fairness in ride-hailing via joint order dispatching and driver repositioning. In *Proceedings of the 28th ACM SIGKDD conference on knowledge discovery and data mining*. 3950–3960.
- [28] Vicente Vivanco Cepeda, Gaurav Kumar Nayak, and Mubarak Shah. 2023. Geolclip: Clip-inspired alignment between locations and images for effective worldwide geo-localization. *Advances in Neural Information Processing Systems* 36 (2023), 8690–8701.
- [29] Chenhao Wang, Lisi Chen, Shuo Shang, Christian S Jensen, and Panos Kalnis. 2024. Multi-Scale Detection of Anomalous Spatio-Temporal Trajectories in Evolving Trajectory Datasets. In *Proceedings of the 30th ACM SIGKDD Conference on Knowledge Discovery and Data Mining*. 2980–2990.
- [30] Yongfu Wei, Yan Lin, Hongfan Gao, Ronghui Xu, Sean Bin Yang, and Jilin Hu. 2025. Path-LLM: A Multi-Modal Path Representation Learning by Aligning and Fusing with Large Language Models. In *Proceedings of the ACM on Web Conference 2025*. 2289–2298.
- [31] Ronghui Xu, Hanyin Cheng, Chenjuan Guo, Hongfan Gao, Jilin Hu, Sean Bin Yang, and Bin Yang. 2025. Mm-path: Multi-modal, multi-granularity path representation learning. In *Proceedings of the 31st ACM SIGKDD Conference on Knowledge Discovery and Data Mining*. 1703–1714.
- [32] Shixiong Xu, Chenghao Zhang, Lubin Fan, Gaofeng Meng, Shiming Xiang, and Jieping Ye. 2024. Addressclip: Empowering vision-language models for city-wide image address localization. In *European Conference on Computer Vision*. Springer, 76–92.

- [33] Peilun Yang, Hanchen Wang, Ying Zhang, Lu Qin, Wenjie Zhang, and Xuemin Lin. 2021. T3s: Effective representation learning for trajectory similarity computation. In *2021 IEEE 37th international conference on data engineering (ICDE)*. IEEE, 2183–2188.
- [34] Sean Bin Yang, Jilin Hu, Chenjuan Guo, Bin Yang, and Christian S Jensen. 2023. Lightpath: Lightweight and scalable path representation learning. In *Proceedings of the 29th ACM SIGKDD Conference on Knowledge Discovery and Data Mining*. 2999–3010.
- [35] Di Yao, Gao Cong, Chao Zhang, and Jingping Bi. 2019. Computing trajectory similarity in linear time: A generic seed-guided neural metric learning approach. In *2019 IEEE 35th international conference on data engineering (ICDE)*. IEEE, 1358–1369.
- [36] Di Yao, Chao Zhang, Zhihua Zhu, Jianhui Huang, and Jingping Bi. 2017. Trajectory clustering via deep representation learning. In *2017 international joint conference on neural networks (IJCNN)*. IEEE, 3880–3887.
- [37] Xie Yu, Jingyuan Wang, Yifan Yang, Qian Huang, and Ke Qu. 2024. BIGCity: A universal spatiotemporal model for unified trajectory and traffic state data analysis. *arXiv preprint arXiv:2412.00953* (2024).
- [38] Daqing Zhang, Nan Li, Zhi-Hua Zhou, Chao Chen, Lin Sun, and Shijian Li. 2011. iBAT: detecting anomalous taxi trajectories from GPS traces. In *Proceedings of the 13th international conference on Ubiquitous computing*. 99–108.
- [39] Hanyuan Zhang, Xingyu Zhang, Qize Jiang, Baihua Zheng, Zhenbang Sun, Weiwei Sun, and Changhu Wang. 2020. Trajectory similarity learning with auxiliary supervision and optimal matching. (2020).
- [40] Wei Zhang, Miaoxin Cai, Tong Zhang, Yin Zhuang, and Xuerui Mao. 2024. Earth-GPT: A universal multimodal large language model for multisensor image comprehension in remote sensing domain. *IEEE Transactions on Geoscience and Remote Sensing* 62 (2024), 1–20.
- [41] Zheng Zhang, Hossein Amiri, Zhenke Liu, Liang Zhao, and Andreas Züfle. 2024. Large language models for spatial trajectory patterns mining. In *Proceedings of the 1st ACM SIGSPATIAL International Workshop on Geospatial Anomaly Detection*. 52–55.
- [42] Jie Zhao, Chao Chen, Yuanshao Zhu, Mingyu Deng, and Yuxuan Liang. 2025. UniTR: A Unified Framework for Joint Representation Learning of Trajectories and Road Networks. In *Proceedings of the AAAI Conference on Artificial Intelligence*, Vol. 39. 13348–13356.
- [43] Ge Zheng, Bin Yang, Jiajin Tang, Hong-Yu Zhou, and Sibe Yang. 2023. Ddcot: Duty-distinct chain-of-thought prompting for multimodal reasoning in language models. *Advances in Neural Information Processing Systems* 36 (2023), 5168–5191.
- [44] Yu Zheng, Hao Fu, Xing Xie, Wei-Ying Ma, and Quannan Li. 2011. *Geolife GPS Trajectory Dataset – User Guide*. Technical Report. Microsoft Research Asia.
- [45] Silin Zhou, Yao Chen, Shuo Shang, Lisi Chen, Bingsheng He, and Shibusaki Ryosuke. 2025. Blurred Encoding for Trajectory Representation Learning. In *Proceedings of the 31st ACM SIGKDD Conference on Knowledge Discovery and Data Mining*.
- [46] Silin Zhou, Shuo Shang, Lisi Chen, Christian S Jensen, and Panos Kalnis. 2024. RED: Effective Trajectory Representation Learning with Comprehensive Information. *arXiv preprint arXiv:2411.15096* (2024).
- [47] Zeyu Zhou, Yan Lin, Haomin Wen, Shengnan Guo, Jilin Hu, Youfang Lin, and Huaiyu Wan. 2024. PLM4Traj: Cognizing Movement Patterns and Travel Purposes from Trajectories with Pre-trained Language Models. *arXiv preprint arXiv:2405.12459* (2024).

A Appendix

A.1 Details of Map-anchored Factors

We define the three components used in the cost function $\text{Cost}(a, b)$ in detail as follows:

- **Motion Homogeneity** ($f_{\text{speed}}(a, b)$). This term measures the internal consistency of movement dynamics within the segment $T_{a,b}$. Specifically, we compute the variance of instantaneous speeds between consecutive GPS points in the segment. A lower variance reflects smoother or more consistent motion, indicating that the segment corresponds to a coherent phase of movement (e.g., cruising or stationary).
- **Route Homogeneity** ($f_{\text{road}}(a, b)$). This term captures the structural consistency of the road types traversed in the segment. We identify the sequence of road IDs that the trajectory crosses, and count the number of transitions between different roads. A smaller number of transitions indicates that the segment is located in a consistent road environment, which is consistent with the intuition that semantic stages should not cross heterogeneous road environments.
- **Segment Length Regularization** ($f_{\text{len}}(a, b)$). In order to avoid generating too short or simple segments, we introduce a regularization term based on segment length. Specifically, $f_{\text{len}}(a, b)$ is defined as the inverse of the number of points from p_a to p_b , which encourages partitions to be long enough to be semantically meaningful while still maintaining internal consistency.

A.2 Details of Semantic Descriptions

This section provides the detailed implementation of the semantic descriptions generated for each sub-trajectory S_n . As outlined in Equation 3, we extract key statistical and dynamic characteristics from the raw GPS points within a sub-trajectory. These features are then formatted into a structured textual template, which serves as a component of the multimodal input for the MLLM.

Time-based Features. For each sub-trajectory S_n , which consists of a sequence of GPS points $\{p_1, \dots, p_k\}$, we extract fundamental temporal information. The **Start Time** is the timestamp of the first point (t_1), the **End Time** is the timestamp of the last point (t_k), and the **Duration** is the total time elapsed, calculated as $(t_k - t_1)$ in seconds.

Distance-based Features. The **Total Distance** of a sub-trajectory is calculated by summing the geographical distances between all consecutive GPS points. We use the Haversine formula to compute the great-circle distance between two points on Earth, ensuring an accurate measurement of the path traveled in meters.

Speed-based Features. To capture the motion dynamics of the sub-trajectory, we compute a set of speed-related metrics. First, we calculate the instantaneous speed between each consecutive pair of points. Based on these values, we derive the following:

- **Average Speed:** Calculated as the Total Distance divided by the total Duration, providing a robust measure of the overall speed in m/s.
- **Maximum Speed:** The highest instantaneous speed recorded between any two consecutive points within the sub-trajectory.

- **Minimum Speed:** The lowest non-zero instantaneous speed recorded within the sub-trajectory.

Textual Template. After computing the features described above, they are populated into a structured, human-readable text template. This format allows the MLLM to easily parse and comprehend the key characteristics of the trajectory segment. An example of the template is shown below:

```
--- Sub-trajectory Segment Description ---
Start Time: 2024-11-01 13:08:36
End Time: 2024-11-01 13:09:42
Duration (seconds): 66
Total Distance (meters): 410.8
Average Speed (m/s): 6.22
Maximum Speed (m/s): 8.51
Minimum Speed (m/s): 1.15
-----
```

A.3 Experimental Settings

This section provides a detailed experimental settings including datasets, task descriptions, baselines, and hyperparameter settings.

A.3.1 Dataset. To evaluate the cross-city generalization and cross-task universality of our framework, we conduct extensive experiments on four large-scale, real-world trajectory datasets, Xi'an, Chengdu, Porto and Geolife.

Table 6: Dataset statistics.

Dataset	Trajectories	Time Span
Chengdu	677,492	2016/11/01 – 2016/11/30
Xi'an	373,054	2016/11/01 – 2016/11/30
Porto	695,085	2013/07/01 – 2014/07/01
Geolife (Beijing)	17,621	2007/04/01 – 2012/08/01

- **Xi'an and Chengdu:** These two datasets contain taxi trajectories collected in Xi'an and Chengdu, China, during October and November 2016. They represent typical urban mobility patterns from ride-hailing services.
- **Porto:** This is a publicly available dataset of taxi trajectories from Porto, Portugal, originally released for a Kaggle competition⁵. Its widespread use in prior research makes it a standard benchmark for comparison.
- **GeoLife:** This dataset, collected by Microsoft Research Asia, contains GPS trajectories from 182 users over several years [44]. The dataset is highly diverse, comprising 17,621 trajectories with a total distance of over 1.2 million kilometers and a duration of more than 50,000 hours. It is ideal for evaluating generalization across different user behaviors and modes of transport.

A.3.2 Tasks Description. We evaluate our framework on four representative downstream tasks that span both regression and classification settings:

- **Travel Time Estimation (TTE):** A regression task to predict the total travel time of a given trajectory. We use Mean Absolute Error (MAE), Root Mean Squared Error (RMSE), and Mean Absolute Percentage Error (MAPE) as evaluation metrics.

⁵<https://www.kaggle.com/c/pkdd-15-predict-taxi-service-trajectory-i>

- **Anomaly Detection (AD):** A binary classification task to identify trajectories that deviate from normal mobility patterns. Following previous work [23], we construct the anomaly dataset and report Accuracy (ACC), Precision (Prec), and the Area Under the Precision-Recall Curve (PR-AUC).
- **Mobility Prediction (MP):** A classification task that predicts the destination region of a trajectory. We use Top-1 Accuracy (ACC@1) and Top-5 Accuracy (ACC@5) for evaluation.
- **Transportation Mode Identification (TMI):** A multi-class classification task on the GeoLife dataset, aiming to identify the mode of transportation. We report Accuracy, Macro-F1, and Weighted-F1.

Ground Truth. Given the scarcity of real-world labeled data for trajectory anomaly detection, we follow previous works [23, 26, 29] and adopt a disturbance-based approach to generate a synthetic anomaly dataset. This involves programmatically injecting two distinct types of anomalies—**detour** and **switch**—into normal trajectories.

- A **detour** is defined by two parameters: an anomaly probability α and a disturbance distance d . For instance, setting $\alpha = 0.1$ and $d = 3$ signifies that 10% of the trajectory's points are displaced by a distance of 3 grid units from their original path.
- **switch** simulates a more drastic deviation, controlled by the trajectory split point μ . An instance with $\mu = 0.3$ indicates that a trajectory follows its original route r_1 for the first 30% of its course, before abruptly switching to an entirely different route r_2 for the remainder of the journey.

In our experiments, the overall proportion of anomaly injection is consistently set to 5%.

A.3.3 Baselines. For each task, we choose three kinds of baselines, *i.e.*, task-specified models, trajectory foundation models and LLM-based models.

Baselines for TTE and MP The baselines for Travel Time Estimation (TTE) and Mobility Prediction (MP) include the following methods:

- **Traj2Vec [36]:** An RNN-based seq2seq model that converts a GPS trajectory into a feature sequence to learn representations, originally for the trajectory clustering task.
- **T2Vec [18]:** A denoising auto-encoder that pre-trains a model by reconstructing original trajectories from their low-sampling-rate counterparts.
- **Trember [7]:** An RNN-based seq2seq model designed to learn trajectory representations by recovering the road segments and timestamps of the input trajectories.
- **CTLE [22]:** A method that pre-trains a bi-directional Transformer with two Masked Language Model (MLM) tasks focusing on location and hour predictions.
- **Toast [2]:** This framework utilizes a context-aware node2vec model to generate road segment representations and trains the model with an MLM-based task and a sequence discrimination task.
- **TrajCL [1]:** A contrastive learning framework that introduces a dual-feature self-attention-based encoder and trains the model in a contrastive style using the InfoNCE loss.

- **MMTEC [21]:** A multi-modal method that learns trajectory representations using an attention-based discrete encoder and a NeuralCDE continuous encoder to extract travel behavior and continuous spatial-temporal correlations.
- **JGRM [24]:** A multi-modal method that learns trajectory representations from the joint perspectives of free-space (GPS) and road networks, using a combination of contrastive loss, MLM loss, and alignment loss.
- **START [10]:** A self-supervised framework that includes a time-aware trajectory encoder and a Graph Attention Network (GAT) and is trained with both an MLM task and a SimCLR-based contrastive task.
- **UniTR [42]:** A unified framework for joint representation learning of road networks and trajectories, which uses a hierarchical propagation mechanism to model their many-to-many interactions and a triple-level contrastive loss for optimization.
- **BLUE [45]:** An encoder-decoder model with a pyramid structure that gradually reduces GPS coordinate precision to create hierarchical patches, thereby capturing both fine-grained details and high-level travel patterns.
- **PLM4Traj [47]:** A model that leverages Pre-trained Language Models (PLMs) for trajectory analysis by incorporating a novel trajectory prompt and a semantic embedder to understand movement patterns and travel purposes.
- **Path-LLM [30]:** A multi-modal path representation learning model that integrates Large Language Models (LLMs) to interpret both topological and textual path data, using contrastive pretraining for alignment and a dynamic fusion module.
- **MM-Path [31]:** A multi-modal, multi-granularity framework designed to learn a generic path representation by systematically aligning and fusing information from both road network-based paths and image-based (e.g., remote sensing) paths.

Baselines for AD For Anomaly Detection (AD), we compare against the following methods:

- **iBAT [38]:** An isolation-based method that detects anomalous trajectories by evaluating how much a target trajectory can be isolated from a set of reference trajectories.
- **GM-VSAE [23]:** A Gaussian mixture variational sequence auto-encoder, which is an RNN-based sequence-to-sequence model that handles complex trajectory distributions by employing a Gaussian mixture model in the latent space.
- **ATROM [8]:** A probabilistic metric learning model that focuses on open anomalous trajectory recognition, aiming to identify which type of anomaly a given trajectory exhibits.
- **DeepTEA [9]:** A state-of-the-art time-dependent method that combines dynamic traffic conditions with trajectory patterns to effectively and efficiently detect online trajectory outliers.
- **MST-OATD [29]:** A multi-scale model designed for online anomalous trajectory detection that considers both spatial and temporal aspects of trajectories to extract features at multiple scales.
- **FOTraj [26]:** An LLM-driven framework for fine-grained and noise-resilient trajectory anomaly detection, which converts trajectories into spatial-temporal graphs and uses a Patch-Gated Robustification (PGR) module to enhance noise resilience.

Baselines for TMI For Transportation Mode Identification (TMI), the baselines are as follows:

- **SECA [3]**: A deep semi-supervised convolutional autoencoder (SECA) architecture that automatically extracts features from GPS segments and leverages both labeled and unlabeled data for classification.
- **TrajODE [20]**: A state-of-the-art method that couples the continuity of Neural Ordinary Differential Equations (ODE) with the robustness of latent variables to model trajectories.
- **TrajFormer [19]**: A transformer-based architecture that generates continuous point embeddings to handle irregular spatial-temporal intervals and uses a squeeze function to improve efficiency for long trajectories.
- **RED [46]**: A self-supervised Transformer-based framework that employs a road-aware masking strategy, a spatial-temporal-user joint embedding scheme, and a dual-objective (next segment prediction and full trajectory reconstruction) to learn comprehensive representations.

A.4 Hyperparameter Analysis

In this section, we analyze the sensitivity of our framework to its key hyperparameter, the context filtering distance threshold θ , which is defined in Equation 5. This parameter is crucial as it controls the amount of contextual information (e.g., POIs, traffic lights) included in the visual representations fed to the MLLM.

The choice of θ involves a critical trade-off. A threshold that is too small may exclude relevant nearby elements that are important for reasoning. For example, in an anomaly detection task as illustrated in Figure 6(a), a restrictive threshold could fail to visualize an existing connecting road. This visual omission might mislead the MLLM to incorrectly perceive the path as disconnected and thus flag a normal trajectory as an anomaly. Conversely, a threshold that is too large can introduce an excessive number of irrelevant elements into the map view. This creates visual clutter and acts as noise, potentially overwhelming the MLLM and degrading its performance.

To investigate this impact empirically, we conducted a sensitivity analysis by varying the value of θ . We evaluated the performance on the Travel Time Estimation (TTE) task, measuring the Mean Absolute Error (MAE). The results of this analysis are illustrated in Figure 6(b).

As shown in Figure 6(b), the model’s performance (lower MAE is better) initially improves as the distance threshold increases from a very restrictive value (e.g., 50m). This is because a larger radius allows the model to incorporate more relevant contextual cues. However, after reaching an optimal point (e.g., 100m for Chengdu and Xian), the performance begins to decline steadily. This trend confirms our hypothesis: overly large values for θ lead to the inclusion of too much irrelevant information, which introduces noise and ultimately hinders the MLLM’s reasoning process.

Based on this analysis, we set θ tailored to the scale of each city’s road network. For the Xian, Chengdu, and Geolife datasets, which feature similarly larger road networks, we selected $\theta_{\text{distance}} = 100$ meters. In contrast, for the Porto dataset with its smaller transportation network, we chose a more constrained value of $\theta_{\text{distance}} = 50$ meters. This approach ensures that each setting strikes an effective

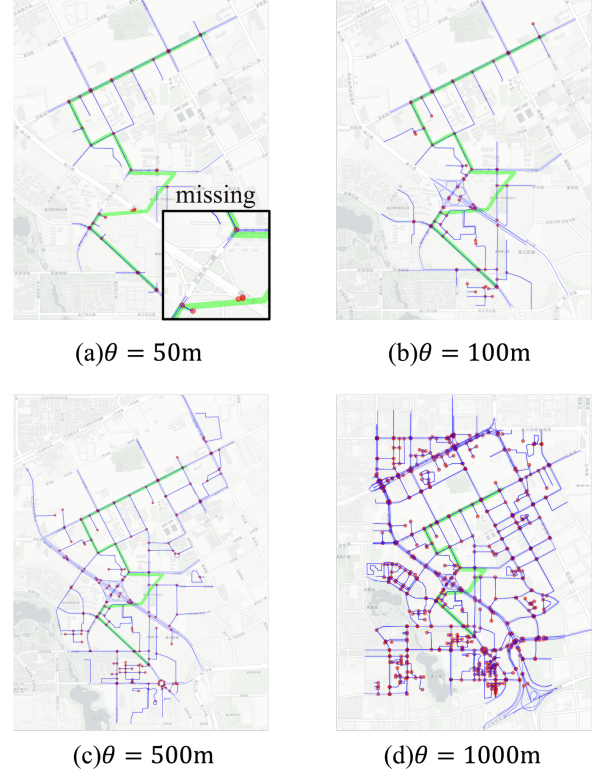


Figure 6: Visual comparison of abnormal trajectories under different distance thresholds.

balance between providing sufficient contextual information while minimizing distracting extraneous elements.

A.5 Reasoning Ability of MLLM’s Outputs

A.5.1 Multi-round reasoning. To further assess the advanced capabilities of Traj-MLLM, we demonstrate its capacity for dynamic, multi-round reasoning. Unlike static models that produce a one-off output, our MLLM-based framework can engage in interactive sessions, adapting its analysis based on new information. We present two case studies drawn from the Travel Time Estimation task, as illustrated in Figure 7. These cases highlight two key abilities: (1) adapting predictions in response to real-time contextual updates, and (2) performing reflective self-correction when presented with ground-truth feedback.

Context-Aware Adaptation to Real-time Events. The first case study demonstrates the model’s ability to adjust its reasoning when provided with new, real-time information. The model initially provides a complete ETA prediction based on the multimodal trajectory data. We then introduce a new piece of information—a traffic accident—to test if the model can correctly locate the event, update its parameters, and recalculate the ETA.

Reflective Self-Correction with Ground Truth. The second case study showcases the model’s ability to reflect on its own prediction error. After the initial prediction is made, we provide the ground-truth arrival time and ask the model to explain the discrepancy.

This mimics a feedback loop where the model can learn and refine its reasoning based on outcomes.

A.5.2 Interpretable Results. A key advantage of our framework is its ability to generate human-readable, interpretable results, leveraging the inherent reasoning capabilities of the MLLM backbone. This goes beyond simply outputting a prediction; the model can articulate the step-by-step logic behind its conclusions, making its outputs transparent and trustworthy. To demonstrate this, we present case studies for our primary downstream tasks, showcasing two core capabilities: sophisticated instruction following and expert-level logical reasoning.

Sophisticated Instruction Following. The MLLM backbone exhibits a remarkable ability to adhere to complex and highly structured instructions defined in the system prompt. This ensures that the model’s output is not only accurate but also consistently formatted, making it reliable for automated pipelines.

- **Case 1: Structured Formatting.** In the Transportation Mode Identification task (Figure 9), the system prompt provides strict formatting rules for the “Final Answer”. It dictates that the answer must appear on a new line after the reasoning and contain *only* the mode name from a predefined list (e.g., ‘train’, ‘walk’, etc.). The output from o4-mini flawlessly adheres to these rules, showcasing its strong instruction-following capabilities.
- **Case 2: Complex Hierarchical Instructions.** The Anomaly Detection task (Figure 8) requires an even more complex, hierarchical output as defined in its system prompt: a “Final Judgment” followed by a three-part “Reasoning” section (Overall Assessment, Evidence Analysis, and Conclusion). As the figure shows, the o4-mini model meticulously follows this multi-level structure, generating a well-organized analytical report that is easy for a human expert to parse. This showcases a high degree of instruction-following capability on complex, nested requirements.

Correctness and Logical Reasoning. More importantly, the model does not just follow formats blindly; it produces correct answers by executing a logical, step-by-step analysis that mimics human expert reasoning. It effectively synthesizes multimodal information to draw sound conclusions.

- **Case 1: Multimodal Synthesis.** In the Transportation Mode Identification task (Figure 9), the model correctly identifies the mode as “train.” Its reasoning demonstrates a powerful synthesis of information: it first uses statistical data (“Speeds (avg 19-24 m/s, max 20-26 m/s) far exceed bike/walk limits”) to eliminate other modes, and then confirms its hypothesis using visual evidence from the user prompt’s images (“the red trajectory exactly overlaps marked railway lines”). This process of elimination and confirmation is a hallmark of robust analytical reasoning.
- **Case 2: Complex Step-by-Step Calculation.** For Travel Time Estimation, the system prompt (Figure 10) instructs the model to act as a navigation expert and perform a detailed, segment-by-segment analysis. The model’s output (Figure 11) shows it executing this complex logic flawlessly. It breaks the journey into four segments, analyzes road characteristics (e.g., “6-lane primary arterial”), traffic flow (“late-night free-flow”), and signal

impacts (“2 signals: 1 at the on-ramp (15s)...”), and then performs explicit calculations (“Running time $1,357 / 17 = 80s$ ”) before summing the results. This demonstrates that the model is performing genuine, step-by-step reasoning rather than simply pattern matching.

To further underscore the advanced reasoning quality of our chosen o4-mini backbone, we provide a qualitative comparison of outputs from different MLLMs for the same anomaly detection task in Figure 12. This comparison reveals that not all models are equally adept at this specialized task. While most models like Gamma-3-27b-it and Gemini-2.5 Pro correctly identify the trajectory as abnormal, their reasoning, though valid, is less precise. For instance, the Gamma-3-12b-it model completely fails, misclassifying the trajectory as “Normal.” In stark contrast, o4-mini provides a diagnosis with expert-level precision, identifying the anomaly not just as a deviation, but as a “translated copy of a side-street path” and a “classic signature of a geometrically shifted (translated) segment.” This superior analytical depth validates our choice of backbone and highlights the effectiveness of our overall framework.

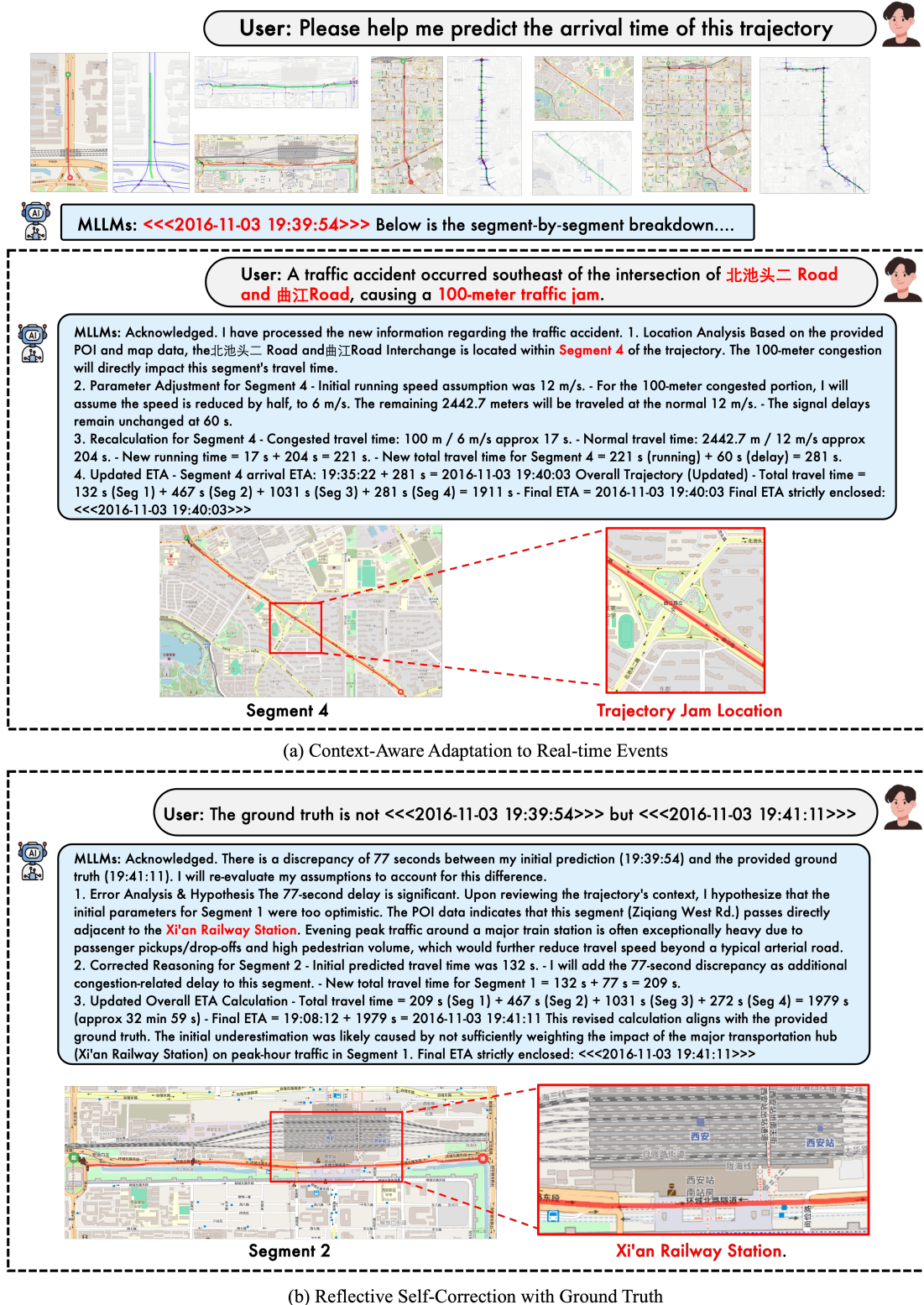


Figure 7: The result of Traj-MLLM.

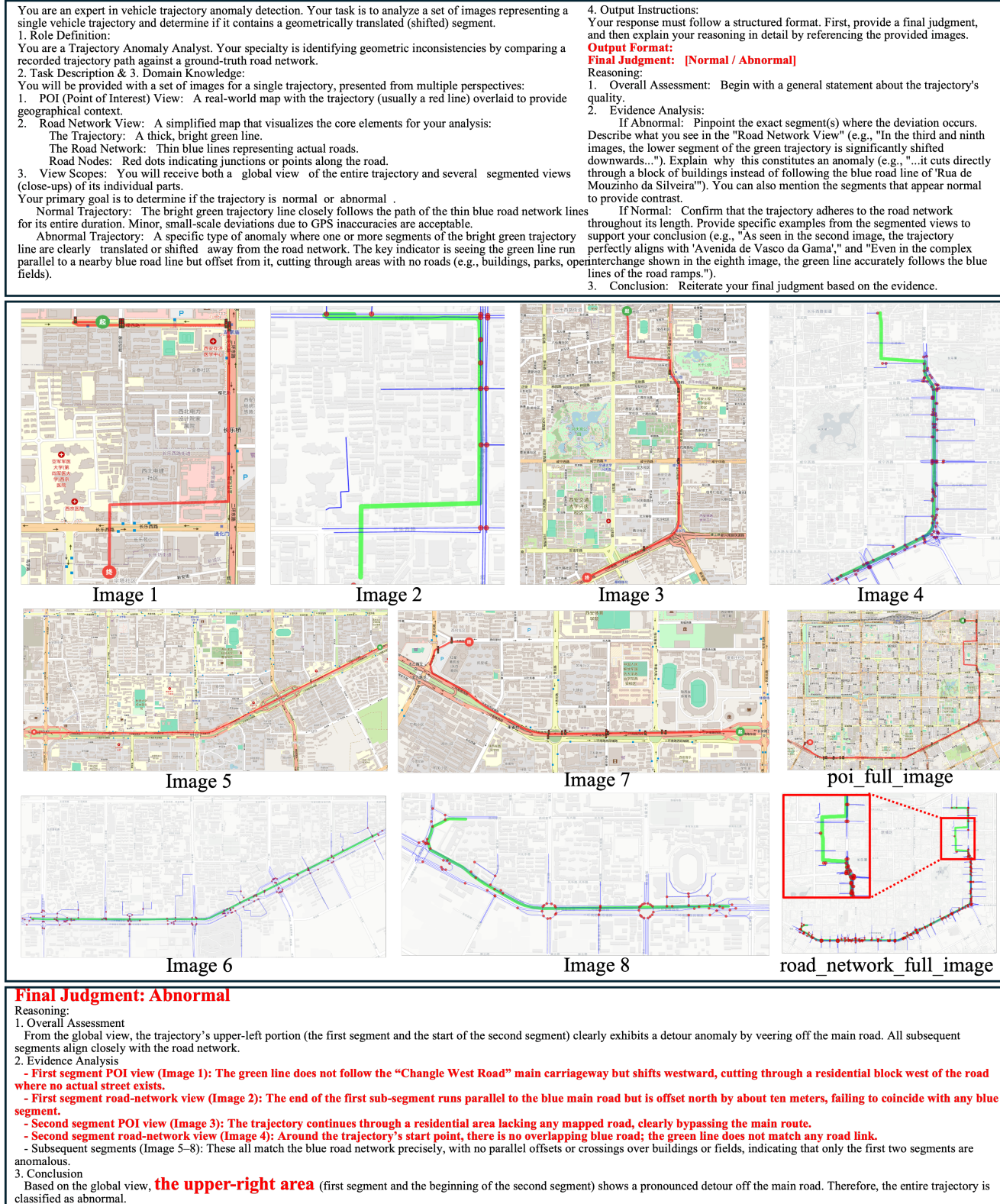


Figure 8: The result of Anomaly Detection. Ground Truth: Anomaly

1. Role Definition

You are an expert in Traffic Mode Classification. Your task is to accurately determine the mode of transport for a given trajectory. The trajectory is provided as a series of chronologically ordered segments, and it's crucial to understand that all segments of a single trajectory share the same, continuous mode of transport.

2. Task Description & 3. Domain Knowledge:

You will receive sequentially segmented trajectory data and corresponding visual information (map screenshots) for each segment. Your goal is to classify the transportation mode for the entire trajectory.

1. Possible Transportation Modes & Constraints:

- walk: Maximum speed = 7 m/s, Maximum acceleration = 3 m/s²
- bike: Maximum speed = 12 m/s, Maximum acceleration = 3 m/s²
- bus: Maximum speed = 34 m/s, Maximum acceleration = 2 m/s²
- car: Maximum speed = 50 m/s, Maximum acceleration = 10 m/s²
- train: Maximum speed = 34 m/s, Maximum acceleration = 3 m/s²

2. Crucial Heuristics for Train Identification:

Railway Overlap: If the red trajectory line in the "POI & Route Detail Map" clearly and consistently overlaps with marked railway lines (often shown as double dashed lines or lines with cross-ties), it is highly probable that the mode is train.

3. General Analysis Guidance:

Analyze both the statistical data (speeds, accelerations) against the provided constraints and the visual information from the maps for each segment.

The consistency of data patterns (e.g., acceleration consistently near a certain limit for a mode) across all segments is a strong indicator, given that the entire trajectory uses a single mode.

Output Formatting:

Your output must consist of two parts:

1. Reasoning: First, provide a brief, bullet-pointed list explaining your decision-making process. Clearly state how you combined the statistical data (e.g., speed, acceleration) and visual information (e.g., railway tracks, road types on the map) to reach your conclusion and rule out other modes.

2. Final Answer: After the reasoning, on a new line, provide the final transportation mode. **This line must ONLY contain the mode name enclosed in triple angle brackets. The mode must be one of the following: 'train', 'walk', 'car', 'bus', 'bike'.**

The trajectory is segmented based on approximate uniformity in traffic semantics.

Below are details for the 4 segments of this trajectory, each with statistical information and corresponding visual data:

Segment 1:

Visuals:

- 'image1' (Shows segment path, POIs, signalized intersections)
- 'image2' (Illustrates road class, lanes, network structure)

Segment Stats:

Start Time: 2008-03-30 17:22:35	End Time: 2008-03-30 17:27:30
Duration (minutes): 4.92	Total Distance (meters): 5733.53
Average Speed (m/s): 19.43	Minimum Speed (m/s): 17.99
Maximum Speed (m/s): 20.64	Maximum Acceleration (m/s ²): 0.0303

Segment 3:

Visuals:

- 'image5' (Shows segment path, POIs, signalized intersections)
- 'image6' (Illustrates road class, lanes, network structure)

Segment Stats:

Start Time: 2008-03-30 17:33:26	End Time: 2008-03-30 17:37:24
Duration (minutes): 3.97	Total Distance (meters): 5033.10
Average Speed (m/s): 21.14	Maximum Speed (m/s): 24.43
Maximum Acceleration (m/s ²): 0.07	Minimum Speed (m/s): 19.67

Overall Trajectory Visuals:

Visuals:

- 'poi_full_image' (Comprehensive view of the entire trajectory with POIs and signalized intersections)
- 'road_structure_full_image' (Detailed illustration of the full trajectory's)

Segment 2:

Visuals:

- 'image3' (Shows segment path, POIs, signalized intersections)
- 'image4' (Illustrates road class, lanes, network structure)

Segment Stats:

Start Time: 2008-03-30 17:28:30	End Time: 2008-03-30 17:32:26
Duration (minutes): 3.93	Total Distance (meters): 4774.46
Average Speed (m/s): 20.23	Maximum Speed (m/s): 26.24
Minimum Speed (m/s): 16.91	Maximum Acceleration (m/s ²): 0.22

Segment 4:

Visuals:

- 'image7' (Shows segment path, POIs, signalized intersections)
- 'image8' (Illustrates road class, lanes, network structure)

Segment Stats:

Start Time: 2008-03-30 17:38:23	End Time: 2008-03-30 17:42:20
Duration (minutes): 3.95	Total Distance (meters): 5750.42
Average Speed (m/s): 24.26	Maximum Speed (m/s): 25.76
Minimum Speed (m/s): 22.37	Maximum Acceleration (m/s ²): 0.047



Image 1

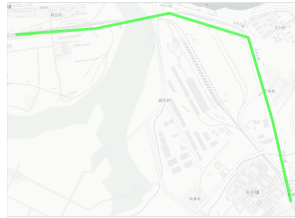


Image 2



Image 3



Image 4

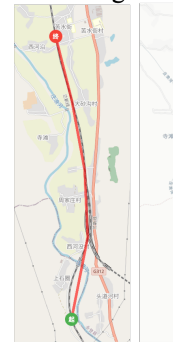


Image 5

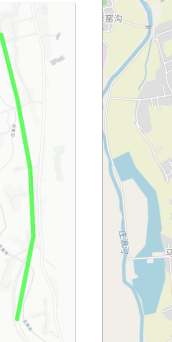


Image 6



Image 7

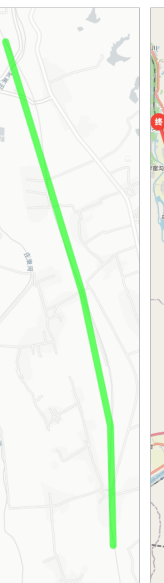
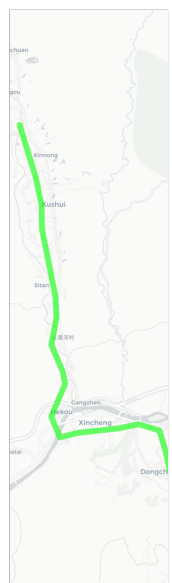


Image 7



poi_full_image



road_structure_full_image

Reasoning:

Speeds (avg ~19–24 m/s, max ~20–26 m/s) far exceed bike/walk limits and are typical of rail service (~70–90 km/h).

Very low, nearly constant accelerations (<0.3 m/s²) and minimal speed variation indicate steady cruise, unlike a car or bus in traffic.

On each segment's POI & Route Detail Map, **the red trajectory exactly overlaps marked railway lines, not roadways.**

The contiguous straight alignment through rural areas following rail infrastructure strongly points to a train.

train

Figure 9: The result of Transportation Mode Identification. Ground Truth: Train

1. Role Definition

You are a premier expert in navigation planning and TTE forecasting, possessing a deep understanding of complex urban traffic dynamics.

2. Task Description

Based on provided segmented trajectory data, map screenshots (detailing POIs, route specifics, and road networks), and vehicle type, you must conduct a detailed, step-by-step analysis to predict the high-precision Estimated Time of Arrival (ETA).

For each trajectory segment, you will:

a. Analyze influencing factors:

- Road Characteristics: Determine road type (highway, arterial, etc.), classification, and speed limits, using visual data like the density of blue OSM lines to interpret road hierarchy.
- Expected Traffic Flow: Estimate traffic levels (e.g., free flow, heavy congestion) based on the time of day and road type.
- Signal Light Impact: Estimate the number of signals and calculate an "average comprehensive delay per signal." This calculation must be probabilistic and context-aware, considering time-of-day, intersection type, road hierarchy, and the possibility of "green waves."

b. Predict the travel time in seconds, clearly justifying your assumed average speed and signal delay values.**c. Predict the average speed in m/s for the segment.****d. Calculate the segment's ETA (YYYY-MM-DD HH:MM:SS).**

Finally, you will synthesize all segment analyses to provide an overall trajectory prediction, culminating in a final ETA.

3. Domain Knowledge

You must leverage built-in expertise in:

- Traffic Regulations: Standard rules of the road and speed limits.
- Congestion Patterns: Typical traffic behavior based on time-of-day (e.g., morning/evening peaks, off-peak, late night) and location.
- Road Type Characteristics: How different roads (highways, arterials, local roads) handle traffic and their typical speed profiles.
- Signal Light Logic: Understanding that traffic signal cycles and delays vary significantly with time-of-day (peak vs. night modes) and intersection hierarchy. For instance, major arterial signals have longer cycles during peak hours, while nighttime may see flashing signals or shorter cycles.
- POI Impact: How Points of Interest can dynamically affect traffic flow.
- Vehicle-Specific Behaviors: Adjusting predictions if the vehicle type (e.g., "Taxi") is specified, accounting for its unique operational patterns.
- Visual Interpretation: Critically, you must interpret road hierarchy from map visuals. A higher density of blue lines (representing OSM road edges) indicates a wider, higher-class road (arterial, expressway), while sparser lines suggest a lower-class road (collector, local).

4. Output Formatting

The final, overall ETA prediction must be strictly enclosed in triple angle brackets.

Example: `<<<2025-05-18 21:35:00>>>`

dynamically_generated_stats_prompt :

The trajectory is segmented based on approximate uniformity in traffic semantics.

Below are details for the 4 segments of this trajectory, each with statistical information and corresponding visual data:

Segment 1:

Visuals:

- `image1` (Shows segment path, POIs, signalized intersections)
- `image2` (Illustrates road class, lanes, network structure)

Segment Stats:

Start Time: 2016-11-03 22:13:27
Distance (meters): 1442.9243 meters

Segment 2:

Visuals:

- `image3` (Shows segment path, POIs, signalized intersections)
- `image4` (Illustrates road class, lanes, network structure)

Segment Stats:

Distance (meters): 2877.617 meters

Segment 3:

Visuals:

- `image5` (Shows segment path, POIs, signalized intersections)
- `image6` (Illustrates road class, lanes, network structure)

Segment Stats:

Distance (meters): 1356.9857 meters

Segment 4:

Visuals:

- `image7` (Shows segment path, POIs, signalized intersections)
- `image8` (Illustrates road class, lanes, network structure)

Segment Stats:

Distance (meters): 2452.5181 meters

Overall Trajectory Visuals:

Visuals:

- `poi_full_image` (Comprehensive view of the entire trajectory with POIs and signalized intersections)
- `road_structure_full_image` (Detailed illustration of the full trajectory's road class, lanes, and network structure)

Figure 10: The system prompt of Travel Time Estimation.

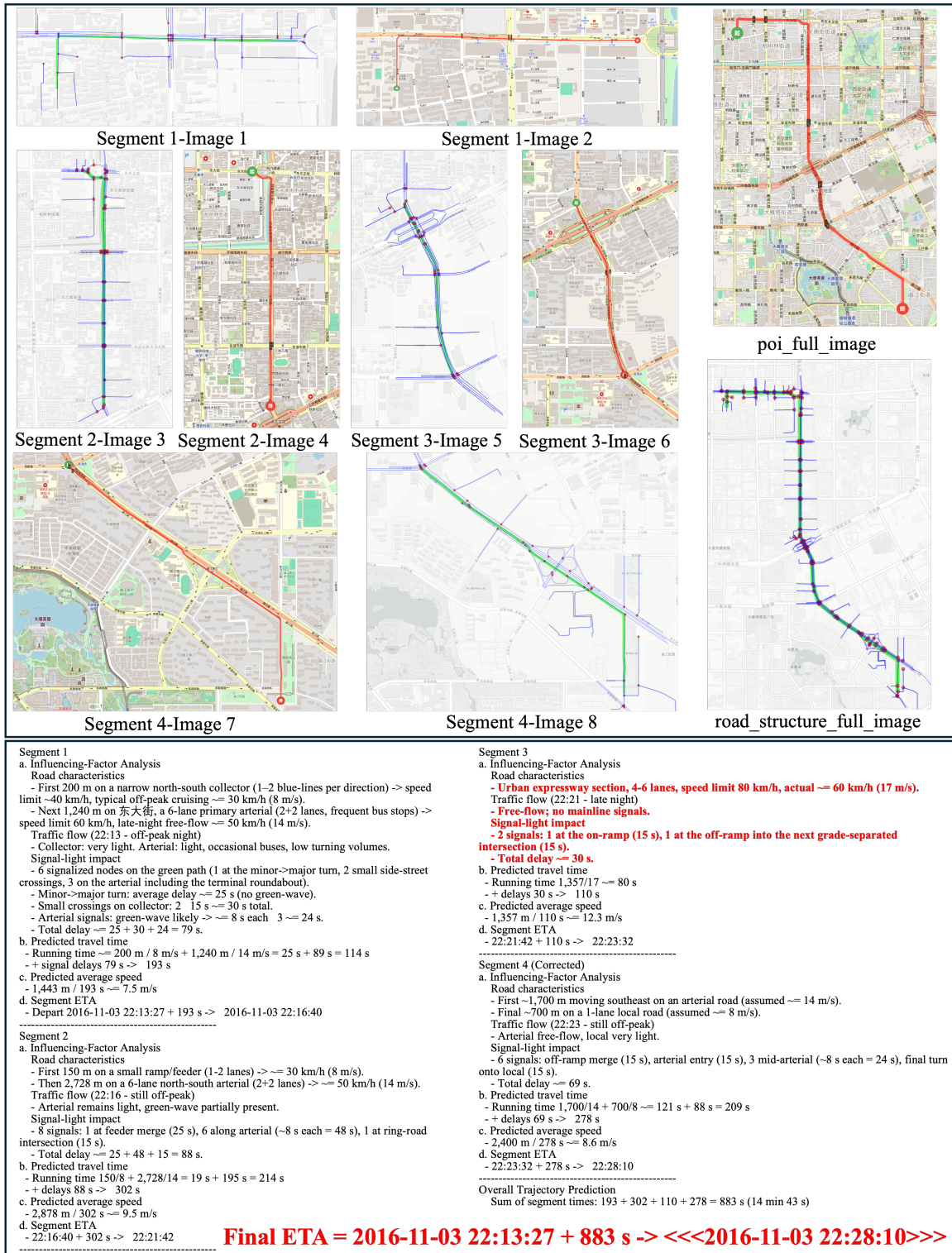


Figure 11: The result of Travel Time Estimation. Ground Truth: 2016-11-03 22:29:01

Gamma-3-4b-it****Final Judgment:** Abnormal******Reasoning:****

1. ****Overall Assessment:**** The trajectory exhibits a clear and consistent anomaly throughout its duration. The green trajectory line frequently deviates significantly from the expected path dictated by the blue road network.
2. ****Evidence Analysis:****
 - * ****Segment 3 (Image 2):**** This is the most prominent example of the anomaly. In the "Road Network View," we can see the trajectory running parallel to 'Rua de Mouzinho da Silveira' but shifted downwards and cutting directly through a large block of buildings. This is a clear case of translation – the trajectory has been moved laterally without any corresponding change in direction. The trajectory is not following the road, but rather traversing an area devoid of roads.
 - * ****Segment 9 (Image 5):**** Another significant deviation occurs in the lower segment of the trajectory. It's running parallel to a blue road, but it's shifted significantly to the right, cutting through a large open area. Again, this demonstrates a geometric translation.
 - * ****Segment 12 (Image 7):**** The trajectory continues to deviate, running parallel to a blue road but offset to the right, passing through an area with buildings.
 - * ****Segments 15 & 16 (Images 8 & 9):**** The trajectory continues to deviate, running parallel to a blue road but offset to the right, passing through an area with buildings.
 - * ****Normal Segments:**** Throughout the trajectory, there are sections where the green line closely follows the blue road network. For example, in the initial portion of the trajectory (Image 1), the green line aligns well with 'Avenida de Vasco da Gama'. Similarly, in the later stages (Image 10), the trajectory generally follows the blue roads, although with minor deviations that are likely due to GPS inaccuracies.
 - * ****Key Indicator:**** The consistent pattern of the green line running parallel to blue roads but offset and cutting through areas without roads is the defining characteristic of this anomaly. It's not a simple curve or a small deviation; it's a systematic translation of the trajectory.
3. ****Conclusion:**** Based on the repeated instances of geometric translation, specifically the trajectory cutting through buildings and open spaces instead of following the road network, the trajectory is classified as abnormal.

Gamma-3-12b-it****Final Judgment:** Normal******Reasoning:****

1. ****Overall Assessment:**** The trajectory, as visualized across the provided images, appears to consistently follow the road network with minimal deviation. While there are some minor variations likely due to GPS inaccuracies, there are no clear instances of geometric translation or shifting away from the established road paths.
2. ****Evidence Analysis:****
 - * The global view (first image) shows the trajectory running along a major arterial road, and it generally aligns with the blue road network lines.
 - * In the second image, the green trajectory closely follows the blue lines representing 'Avenida de Vasco da Gama'.
 - * The third image, depicting a complex interchange, demonstrates that the green trajectory accurately navigates the road ramps and junctions, aligning with the blue road network.
 - * The fourth image shows the trajectory following the road network along a straight section.
 - * The fifth image shows the trajectory following the road network through a complex intersection.
 - * The sixth image shows the trajectory following the road network along a straight section.
 - * The seventh image shows the trajectory following the road network through a complex intersection.
 - * The eighth image shows the trajectory following the road network along a straight section.
 - * The ninth image shows the trajectory following the road network along a straight section.
 - * The tenth image shows the trajectory following the road network along a straight section.
 - * The eleventh image shows the trajectory following the road network along a straight section.
 - * The twelfth image shows the trajectory following the road network along a straight section.
3. ****Conclusion:**** Based on the consistent alignment of the green trajectory with the blue road network across all provided images, I conclude that the trajectory is ****normal****. There is no evidence of a geometrically translated or shifted segment.

Gamma-3-27b-it****Final Judgment:** Abnormal******Reasoning:****

1. ****Overall Assessment:**** The trajectory exhibits significant deviations from the road network in several segments, indicating a clear anomaly. While portions of the trajectory follow roads reasonably well, there are distinct instances of geometric translation.
2. ****Evidence Analysis:****
 - * In the fourth and seventh images, the green trajectory line diverges sharply from the blue road network. Specifically, the green line cuts across open areas and appears to run parallel to, but offset from, the roads. This is a clear indication of a translated segment. The green line is not following any existing road infrastructure in these areas.
 - * The eighth image also shows a significant deviation. The green line splits into two parallel segments, both of which are offset from the blue road network. This is a clear indication of a geometric anomaly.
 - * In contrast, the initial segments shown in the first three images appear relatively normal, with the green line generally following the blue road lines. Similarly, the final segment in the tenth image appears to adhere to the road network. However, these normal segments do not negate the significant anomalies observed in the middle sections.
3. ****Conclusion:**** Based on the clear evidence of geometric translation and offset segments, particularly in images four, seven, and eight, the trajectory is definitively abnormal. The observed deviations cannot be attributed to minor GPS inaccuracies and represent a significant anomaly in the vehicle's path.

o4-mini

Final Judgment: Abnormal

Reasoning:

1. Overall Assessment
 - Most of the trajectory—especially the long straight run along the main north–south artery—closely adheres to the mapped road and shows only minor GPS jitter. However, one short segment clearly deviates as a translated copy of a side-street path.
2. Evidence Analysis
 - The global Road-Network View (fourth image) shows the trajectory in bright green superimposed on the true road graph in blue. The bulk of the journey runs exactly down the central blue spine road.
 - In the detailed segment views (seventh and eighth images):
 - * You can see where the vehicle leaves the main road (the green line turns east). The real eastward street is drawn in blue just north of the point where the green segment starts, but instead of lining up, the green line is shifted about 30–50 m too far south. It cuts straight across a block of buildings (no blue road underneath).
 - * Then, as the vehicle should turn north onto a secondary street, the green path again is parallel to that street's blue centerline but offset to the east, crossing open space rather than following the street.
 - * Beyond that patch, the green trajectory "snaps back" to the correct road network and realigns with the blue lines.
 - This pattern—a series of points that match the shape of an actual turn but are all translated off the true road by a consistent offset—is the classic signature of a geometrically shifted (translated) segment.
3. Conclusion
 - Because a distinct portion of the trip is clearly running parallel to nearby streets yet displaced into areas without roads, the trajectory contains a translated/shifted segment and must be labeled Abnormal.

Gemini-2.5 Pro****Final Judgment:** Abnormal******Reasoning:****

1. ****Overall Assessment:**** While the majority of this trajectory demonstrates a high degree of accuracy by following the road network closely, its final segment contains a clear and significant geometric translation anomaly.
2. ****Evidence Analysis:****
 - * ****If Abnormal:**** The anomaly is located at the end of the trajectory. The global views (images 4 and 5) already suggest a deviation near the destination point. The conclusive evidence is found in the final segmented views.
 - * ****Image 10 (Road Network View):**** This image provides the clearest proof of the anomaly. After following the main road (represented by the dense blue lines and red nodes) for most of its path, the bright green trajectory makes an abrupt right turn, travels eastward across an open area where there are no corresponding blue road lines, and then makes another turn to connect to a different road. This segment runs parallel to the actual road network but is clearly shifted, cutting through what appears to be a residential or commercial block.
 - * ****Image 3 (POI View):**** This real-world map view corroborates the finding. The red trajectory line is shown leaving the main thoroughfare (一环路东一段) and cutting diagonally through a block of buildings to reach the endpoint near 桃蹊路. This path does not follow any mapped road.
 - * ****Contrasting Normal Segments:**** In contrast, the initial and middle portions of the trajectory are normal. For example, in Image 2 and Image 9, the bright green trajectory line is perfectly centered on the thin blue road network lines, indicating an accurate recording for those sections. This makes the deviation in the final segment even more pronounced.
3. ****Conclusion:**** The presence of a distinct segment where the trajectory is geometrically shifted away from the ground-truth road network makes this an ****abnormal**** trajectory. The vehicle did not follow this recorded path; rather, the data for this final segment was erroneously translated.

Figure 12: Qualitative comparison of outputs from different MLLM backbones for the Anomaly Detection task. The same input was provided to each model.